NONCONFORMING DOMAIN DECOMPOSITION TECHNIQUES FOR LINEAR ELASTICITY

ROLF H. KRAUSE* AND BARBARA I. WOHLMUTH†

Abstract. Mortar finite element methods provide a powerful tool for the numerical approximation of partial differential equations. Many domain decomposition techniques based on the coupling of different discretization schemes or of nonmatching triangulations along interior interfaces can be analyzed within this framework. Here, we present a mortar formulation based on dual basis functions and a special multigrid method. The starting point for our multigrid method is a symmetric positive definite system on the unconstrained product space. In addition, we introduce a new algorithm for the numerical solution of a nonlinear contact problem between two linear elastic bodies. It will be shown that our method can be interpreted as an inexact Dirichlet–Neumann algorithm for the nonlinear problem. The boundary data transfer at the contact zone is essential for the algorithm. It is realized by a scaled mass matrix which results from a mortar discretization on non–matching triangulations with dual basis Lagrange multipliers. Numerical results illustrate the performance of our approach in 2D and 3D.

Key words. mortar finite elements, Lagrange multiplier, dual space, non–matching triangulations, multigrid methods, contact problems, linear elasticity

AMS subject classifications. 65N30, 65N55, 74B10

1. Introduction.

We present domain decomposition methods within the framework of mortar techniques [BMP93, BMP94]. Originally introduced as a nonconforming method for the coupling of spectral elements, these techniques can be used in a large class of situations. The coupling of different physical models, discretization schemes or non–matching triangulations along interior interfaces of the domain can be analyzed by mortar methods. These domain decomposition techniques provide a more flexible approach than standard conforming formulations, and are of special interest for time dependent problems, rotating geometries, inhomogeneous materials, problems with local anisotropies, corner singularities, contact problems and when different terms dominate in different regions of the simulation domain. One major requirement to obtain optimal discretization schemes is that the interfaces between the different regions are handled appropriately, see, e.g., [BD98, Ben99, BMP93, BMP94]. Very often, suitable matching conditions at the interfaces can be formulated as weak continuity conditions. Here, we consider mortar finite element formulations based on a dual basis for the Lagrange multiplier space, see [Woh00], with special emphasis on nonlinear contact problems. As a consequence of the biorthogonality relation and in contrast to the standard mortar methods, the locality of the support of the nodal basis functions of the corresponding constrained space is preserved. Based on this observation, we analyze a modified multigrid method and present numerical results in 2D and 3D illustrating the performance of the iterative solver, see [WK01]. As application, we choose the deformation of linear elastic bodies, and we consider composite materials, see [KW00b, KW00a] for the linear case. In this case, the actual zone of contact between the bodies is known in advance. The resulting discrete problem is

* Institut für Mathematik I, Freie Universität Berlin, Arnimallee 2, D–14195 Berlin, Germany
Email: krause@math.fu-berlin.de, http://www.math.fu-berlin.de/~krause
†Math. Institut, Universität Augsburg, Universitätsstr. 14, D–86159 Augsburg, Germany.
Email: wohlmuth@math.uni-augsburg.de, http://wwwhoppe.math.uni-augsburg.de/~wohlmuth
This work was supported in part by the RiP program of the Mathematisches Forschungsinstitut Oberwolfach which is financed by the Volkswagen–Stiftung

linear and can be solved efficiently by a modified variant of our multigrid method. Here, we introduce suitable locally defined rotations.

Moreover, we focus on a nonlinear problem modeling the contact of two linear elastic bodies. Here, the actual zone of contact is not known in advance and has to be identified during the iteration process. A lot of work has been done on contact problems, see, e.g., [DNS99, WG97, HH80, HH81, ESW99] and [Wri95, IHL88, KO88] for survey papers. Two main difficulties occur in the numerical simulation of contact problems. The first is the handling of the boundary data transfer at the interface between the two bodies. In our setting, this information transfer is realized in terms of the scaled mass matrix from the mortar formulation. The second difficulty is the intrinsic nonlinearity of the problem at the contact boundary. To overcome this difficulty, we use a monotone multigrid method as a subdomain solver, see [Kor97a, KK99, KK00]. This method provides an efficient iterative scheme for elliptic obstacle problems but cannot be applied efficiently to multi body problems with non–matching triangulations. Using mortar techniques for the discretization and a monotone multigrid method as subdomain solver, we introduce a new algorithm for the numerical solution of contact problems. It can be interpreted as a nonlinear Dirichlet–Neumann type preconditioner.

The rest of the paper is organized as follows: In Section 2, we apply mortar techniques to linear elasticity problems. We briefly discuss the idea of a dual basis for the Lagrange multiplier space, and we recall the mortar formulation. Piecewise constant and piecewise linear dual basis functions are given in 2D and for hexahedral triangulations in 3D. We focus on a new mortar formulation on the unconstrained product space in Section 3. It is defined in terms of a local projection operator based on a dual Lagrange multiplier space. In Section 4, we present our multigrid method. Level independent convergence rates are obtained for the $\mathcal{W}$–cycle provided that the number of smoothing steps is large enough. The grid transfer operators have to be modified by a local projection. Numerical results illustrate, in Section 5, the performance of our multigrid method in 2D and 3D. Section 6 shows the flexibility of the mortar approach combined with the concept of dual basis functions. The coupling condition at the interface is weakened, and free displacement in tangential direction is permitted. The main result of our paper can be found in Section 7. We consider a nonlinear contact problem for two linear elastic bodies and present a nonlinear Dirichlet–Neumann algorithm. In each iteration step, we have to solve a linear Neumann problem and a nonlinear one–sided contact problem with given obstacle. Numerical examples show the deformation of the bodies and the stresses at the contact zone.

2. Dual Lagrange multiplier spaces and mortar formulation. We consider the deformation of a body of hyperelastic Hookean material as model problem. The body in its reference configuration is identified with the domain Ω in $\mathbb{R}^d$. The displacement field $\mathbf{u}$ of the body is given as the solution of the following boundary value problem

$$\begin{aligned} -\sigma_{ij}(\mathbf{u})_{,j} &= f_i, && \text{in } \Omega\,, \\ \mathbf{u} &= 0, && \text{on } \Gamma_D\,, \\ \sigma_{ij}(\mathbf{u}) \cdot n_j &= p_i, && \text{on } \Gamma_F\,, \end{aligned}$$

where we assume Ω to be a bounded, polyhedral domain in $\mathbb{R}^d$, $d = 2, 3$, and $\mathbf{n}$ is the unit outer normal on the boundary of Ω. The volume forces are denoted by $\mathbf{f} \in (L^2(\Omega))^d$, and $\mathbf{p} \in (L^2(\Gamma_F))^d$ are the surface stresses. We denote vector quantities

by bold symbols, e.g., $\mathbf{v}$, and its i–th component by v_i. The partial derivative with respect to x_j is abbreviated with the index $_{,j}$. Furthermore, we enforce the summation convention on all repeated indices ranging from 1 to d. The stress tensor σ is given by Hooke's law

$$\sigma_{ij}(\mathbf{u}) := E_{ijlm}\, u_{l,m}\,,$$

where Hooke's tensor $E := (E_{ijlm})_{i,j,l,m=1}^{d}$, $E_{ijlm} \in L^\infty(\Omega)$, is assumed to be sufficiently smooth, symmetric, i.e., $E_{ijlm} = E_{jilm} = E_{lmij}$, $1 \le i,j,l,m \le d$, and uniformly positive definite, i.e., $E_{ijlm}\xi_{ij}\xi_{lm} \ge c\,\xi_{ij}\ \xi_{ij}$ for each symmetric tensor ξ, $\xi_{ij} = \xi_{ji}$. For homogeneous isotropic materials, Hooke's tensor depends only on the Poisson ratio ν and Young's modulus E. Then, the stress tensor can be written as

$$\sigma_{ij}(\mathbf{u}) = \frac{E\ \nu}{(1+\nu)(1-2\nu)}\delta_{ij}\epsilon_{kk}(\mathbf{u}) + \frac{E}{1+\nu}\epsilon_{ij}(\mathbf{u})\,,$$

where $\epsilon(\mathbf{u}) := \frac{1}{2}(\nabla\mathbf{u}^T + \nabla\mathbf{u})$ is the linearized strain tensor. The boundary $\partial\Omega = \overline{\Gamma}_D \cup \overline{\Gamma}_F$ is decomposed into two non–overlapping parts, a Dirichlet part Γ_D with non zero measure and a Neumann part Γ_F. Let $\mathbf{u} \in \mathbf{H}^1_*(\Omega)$ be the solution of the following variational problem

$$a(\mathbf{u},\mathbf{v}) \ = \ f(\mathbf{v}), \quad \mathbf{v} \in \mathbf{H}^1_*(\Omega)\,, \tag{2.1}$$

where $\mathbf{H}^1_*(\Omega)$ is a subspace of $\mathbf{H}^1(\Omega) := (H^1(\Omega))^d$ given by

$$\mathbf{H}^1_*(\Omega) \ := \ \left\{\mathbf{v} \in \mathbf{H}^1(\Omega)\,|\quad \mathbf{v}|_{\Gamma_D} = 0\right\},$$

and $f(\mathbf{v}) := (\mathbf{v},\mathbf{f})_{0;\Omega} + (\mathbf{v},\mathbf{p})_{0;\Gamma_F}$. The bilinear form $a(\cdot,\cdot)$ is defined as

$$a(\mathbf{w},\mathbf{v}) \ := \ \int_\Omega E_{ijlm} w_{i,j} v_{l,m}\, dx, \quad \mathbf{w},\mathbf{v} \in \mathbf{H}^1(\Omega)\,.$$

Associated with $a(\cdot,\cdot)$ is the energy norm $|||\cdot|||$, $|||\mathbf{v}|||^2 := a(\mathbf{v},\mathbf{v})$. Korn's inequality yields the unique solvability of the variational problem (2.1).

We assume that the domain Ω has been decomposed into K non–overlapping polyhedral subdomains Ω_k, $\overline{\Omega} = \bigcup_{k=1}^K \overline{\Omega}_k$, and $\Omega_l \cap \Omega_k = \emptyset$, $k \ne l$. Each subdomain Ω_k is associated with a family of shape regular triangulations $\mathcal{T}_{h_k}$, $h_k \le h_{k;0}$, where h_k is the maximum of the diameters of the elements in $\mathcal{T}_{h_k}$. We use Lagrangian conforming finite elements $S(\Omega_k,\mathcal{T}_{h_k}) \subset H^1(\Omega_k)$ of order one on the individual subdomains and enforce homogeneous Dirichlet boundary conditions on $\Gamma_D \cap \partial\Omega_k$. For the moment, we restrict ourselves to the geometrical conforming situation where the intersection between the boundary of any two different subdomains $\partial\Omega_l \cap \partial\Omega_k$, $k \ne l$, is either empty, a vertex, a common edge in 2D or face in 3D. Furthermore, we assume that the interfaces in 3D are axiparallel rectangulars.

To obtain an optimal discretization scheme, one has to impose suitable matching conditions at the interfaces. In [BMP93, BMP94], it has been shown that weak constraints across the interfaces are sufficient to guarantee approximation and consistency errors of optimal order. The mortar method is characterized by introducing Lagrange multiplier spaces given on the interfaces, which are used to "glue" the different parts of the weak solution together. A suitable triangulation on the interfaces is necessary for the definition of a discrete Lagrange multiplier space. Each interface $\partial\Omega_l \cap \partial\Omega_k$

is associated with a $(d-1)$–dimensional mesh, inherited either from $\mathcal{T}_{h_k}$ or from $\mathcal{T}_{h_l}$. In general, these triangulations do not coincide, see Figure 2.1. The interfaces are denoted by γ_m, $1 \le m \le M$. For each interface, there exists a couple $1 \le l < k \le K$ such that $\overline{\gamma}_m = \partial\Omega_l \cap \partial\Omega_k$. The elements of the $(d-1)$–dimensional mesh on γ_m are boundary edges in 2D or boundary faces in 3D of $\mathcal{T}_{h_l}$ or $\mathcal{T}_{h_k}$. The choice is arbitrary but fixed. Then, the non–mortar side is the one from which the Lagrange multiplier space inherits its mesh, see Figure 2.1. The adjacent side is called mortar side. We denote the set of vertices on the non–mortar side in the interior of γ_m by $\mathcal{P}_m$.

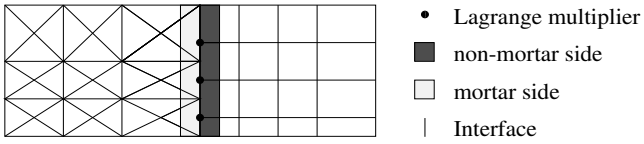

FIG. 2.1. *Non–matching triangulations at the interface*

In the rest of this section, we consider the saddle point formulation of the mortar method using dual spaces. It is defined on the unconstrained product space and a suitable Lagrange multiplier space. A standard choice for the Lagrange multiplier space on each interface is a modified trace space on the non–mortar side, [BMP93, BMP94]. Here, we work with dual basis functions. In both cases, the dimension is equal to the number of vertices in $\mathcal{P}_m$, and optimal a priori estimates can be obtained for the discretization error in the energy norm.

2.1. Dual basis functions. In this subsection, we briefly review the definition of dual basis functions for the scalar Lagrange multiplier space $M_h(\gamma_m)$ associated with the interface γ_m, see [Woh00]. The nodal basis functions μ_p, $p \in \mathcal{P}_m$, are locally defined, piecewise constant or linear and satisfy the following biorthogonality relation

$$\int_{\gamma_m} \mu_p \phi_{p'}\, ds = \delta_{p,p'} \int_{\gamma_m} \phi_{p'}\, ds, \quad p, p' \in \mathcal{P}_m\,, \tag{2.2}$$

where ϕ_p is the standard conforming nodal basis function of $S(\Omega_{n(m)}, \mathcal{T}_{h_{n(m)}})$ associated with the vertex p, i.e., $\phi_p(p') = \delta_{p,p'}$. Here, $n(m)$ is the subdomain index of the non–mortar side of γ_m. Figure 2.2 shows piecewise linear and piecewise constant dual basis functions in 2D at the interface.

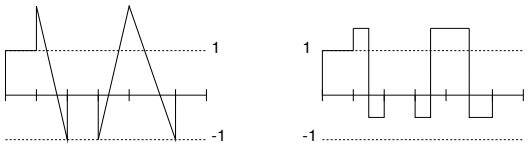

FIG. 2.2. *Piecewise linear and piecewise constant dual basis functions in 2D*

We observe that the basis functions associated with the vertices adjacent to the endpoints of γ_m have to be modified. Figure 2.3 illustrates the isolines of the dual basis function μ_p in 3D restricted to its support in the case of a hexahedral triangulation. We remark that the support of a nodal dual basis function is the union of four boundary faces of $\mathcal{T}_{h_{n(m)}}$ sharing one vertex. As in the 2D case, the definition of μ_p has to be modified if the vertex p is close to the boundary of γ_m, see [BD98, WK01, Woh99a]

for more details. In the case of a simplicial triangulation, the construction follows the same lines, and we refer to [BD98, KLPV00, Woh99a] for details.

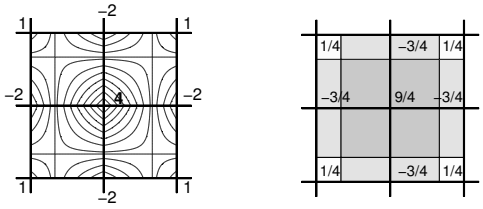

FIG. 2.3. *Isolines of piecewise bilinear and piecewise constant dual basis functions in 3D*

Figure 2.4 shows the modifications in the neighborhood of the boundary of γ_m for piecewise bilinear dual basis functions. We distinguish between three different types of vertices $p \in \mathcal{P}_m$. The inner ones, i.e., $\partial \operatorname{supp}(\phi_p|_{\gamma_m}) \cap \partial\gamma_m = \emptyset$, are marked with empty squares, the ones close to the corners, i.e., $\partial \operatorname{supp}(\phi_p|_{\gamma_m})$ contains one corner of γ_m, by empty circles, and all other vertices are marked by filled circles. In the left of Figure 2.4, the different groups of vertices are shown. For each vertex type, one dual basis function is given in the right part of Figure 2.4. The other ones can be obtained by rotations of $\pi/2$. We observe that the dual basis functions in 3D reflect the tensor product structure of the triangulation, i.e., they can be written as the product of two piecewise linear dual basis functions in 1D.

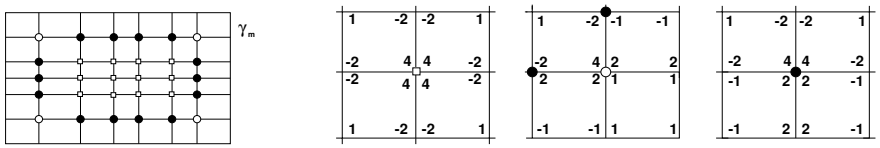

FIG. 2.4. *Modifications near the boundary of γ_m for piecewise bilinear dual basis functions*

Optimal a priori estimates for the discretization error in both the L^2– and H^1–norm as well as for the Lagrange multiplier in the $H_{00}^{1/2}$–dual norm and a weighted L^2–norm are obtained for scalar elliptic equations [Woh99a].

2.2. Mortar formulation. We consider two different types of coupling at the interfaces. The first one is the weak coupling of the solution in both, normal and tangential, directions. In this situation, the different bodies or materials are glued together, i.e., there is no relative displacement in tangential and normal direction. The second interesting case can be used for the modeling of a contact problem and will be discussed in Section 6. In that case, we do not have a weak continuity condition in tangential direction. The constraints at the interfaces are given for the displacements in normal direction. Both situations will be considered within the mortar framework, and the resulting systems will be solved by a modified multigrid method.

The unconstrained product space associated with the domain decomposition is given by

$$\mathbf{X}_h := \prod_{k=1}^{K} (S(\Omega_k, \mathcal{T}_{h_k}))^d .$$

In the case of the coupling in tangential and normal direction, the Lagrange multiplier

space $\mathbf{M}_h$ is also vector valued

$$\mathbf{M}_h := \prod_{m=1}^{M} (M_h(\gamma_m))^d,$$

where $M_h(\gamma_m)$ is spanned by the dual basis functions μ_p, $p \in \mathcal{P}_m$, given in the previous subsection. Now, the mortar formulation is defined in terms of the bilinear form $b(\cdot,\cdot)$

$$b(\mathbf{v},\boldsymbol{\mu}) = \sum_{m=1}^{M} \langle [v_i], \mu_i \rangle_{\gamma_m}, \quad \mathbf{v} \in \mathbf{X}_h, \boldsymbol{\mu} \in \mathbf{M}_h .$$

Here, $[\cdot]$ denotes the jump, i.e., $[v_i]|_{\gamma_m} := v_i|_{\Omega_{n(m)}} - v_i|_{\Omega_{\overline{n}(m)}}$, where $n(m)$ is the subdomain index of the non–mortar side and $\overline{n}(m)$ the index of the adjacent mortar side, and $\langle\cdot,\cdot\rangle_{\gamma_m}$ stands for the duality pairing between $H^{1/2}(\gamma_m)$ and its dual space. Introducing the Lagrange multiplier as an additional unknown, we obtain the following saddle point problem: Find $(\mathbf{u}_h, \boldsymbol{\lambda}_h) \in \mathbf{X}_h \times \mathbf{M}_h$ such that

$$\begin{aligned} a(\mathbf{u}_h,\mathbf{v}) + b(\mathbf{v},\boldsymbol{\lambda}_h) &= f(\mathbf{v}), & \mathbf{v} &\in \mathbf{X}_h , \\ b(\mathbf{u}_h,\boldsymbol{\mu}) &= 0, & \boldsymbol{\mu} &\in \mathbf{M}_h , \end{aligned} \tag{2.3}$$

see [Ben99] for the scalar elliptic case. Here, the bilinear form $a(\cdot,\cdot)$ is extended to the nonconforming space $\mathbf{X}_h$ by replacing the integral over Ω by its broken form $\sum_{k=1}^{K} \int_{\Omega_k}$. The second equation of the saddle point problem guarantees the weak continuity of the solution $\mathbf{u}_h$. We define the nonconforming space $\mathbf{V}_h$ as the kernel of the operator $B^T : \mathbf{X}_h \longrightarrow \mathbf{M}_h$ associated with the bilinear form $b(\cdot,\cdot)$,

$$\mathbf{V}_h := \{\mathbf{v} \in \mathbf{X}_h \mid b(\mathbf{v},\boldsymbol{\mu}) = 0,\ \boldsymbol{\mu} \in \mathbf{M}_h\}.$$

Under the assumption that $a(\cdot,\cdot)$ is uniformly elliptic on $\mathbf{V}_h \times \mathbf{V}_h$, i.e.,

$$a(\mathbf{v},\mathbf{v}) \geq c\,\|\mathbf{v}\|_1^2 := \sum_{k=1}^{K} \|\mathbf{v}\|_{1;\Omega_k}^2, \quad \mathbf{v} \in \mathbf{V}_h ,$$

the following variational problem has a unique solution: Find $\mathbf{u}_h \in \mathbf{V}_h$ such that

$$a(\mathbf{u}_h,\mathbf{v}) = f(\mathbf{v}), \quad \mathbf{v} \in \mathbf{V}_h . \tag{2.4}$$

In the next subsection, we address the question of ellipticity. A uniform discrete inf–sup condition yields in combination with the ellipticity of $a(\cdot,\cdot)$ on the kernel of the operator B^T the unique solvability of (2.3), see [BF91]. We refer to [Woh99a] for the proof of the inf–sup condition in the scalar case. Since $\mathbf{M}_h$ and $\mathbf{X}_h$ are product spaces, the inf–sup condition follows from the scalar case. Moreover, the positive definite system (2.4) is equivalent to the saddle point problem (2.3).

2.3. Uniform ellipticity. In this section, we consider the uniform ellipticity of the bilinear form $a(\cdot,\cdot)$ on the constrained space $\mathbf{V}_h \times \mathbf{V}_h$. Let us start with the special case that $\partial\Omega_k \cap \Gamma_D$ has a non zero measure for all $1 \leq k \leq K$. In this situation, Korn's inequality can be applied to each subdomain, and we find

$$a(\mathbf{v},\mathbf{v}) = \sum_{k=1}^{K} a_k(\mathbf{v},\mathbf{v}) \geq C \sum_{k=1}^{K} \|\mathbf{v}\|_{1;\Omega_k}^2 = C\|\mathbf{v}\|_1^2, \qquad \mathbf{v} \in \mathbf{X}_h ,$$

where $a_k(\cdot,\cdot)$ stands for the restriction of $a(\cdot,\cdot)$ to the subdomain Ω_k. We remark that C does not depend on the number of subdomains. Here, we use standard Sobolev notations for the norms and seminorms and the constants $0 < c, C < \infty$ are generic ones not depending on the meshsize. Unfortunately, many interesting cases do not satisfy this assumption. However for the unique solvability of (2.4), it is sufficient to have the uniform ellipticity of $a(\cdot,\cdot)$ on $\mathbf{V}_h \times \mathbf{V}_h$. In the scalar elliptic case, the kernel of the corresponding bilinear form is the subspace of piecewise constant functions. The dimension is given by the number of subdomains Ω_k such that $\partial\Omega_k \cap \Gamma_D$ is empty. In our setting, the kernel is of higher dimension. The rigid body motions per subdomain define a three dimensional space in 2D and a six dimensional space in 3D. Thus, the dimension of the Lagrange multiplier space has to be larger than d. In the following, we assume that $\#\mathcal{P}_m \geq 2$ in 2D, and that in 3D the triangulation at the interface is a tensor product mesh with $\#\mathcal{P}_m \geq 4$.

To prove the uniform ellipticity in the scalar elliptic case, it is sufficient to show that the constants are contained in the Lagrange multiplier space. Due to the rigid body motions this is not sufficient in our case. To get a better feeling for the kernel of $a(\cdot,\cdot)$, we consider the case of two unit squares Ω_1 and Ω_2 with homogeneous Dirichlet boundary condition on one side of $\partial\Omega_1 \cap \partial\Omega$ and homogeneous Neumann boundary condition elsewhere. Then, $a(\cdot,\cdot)$ is not elliptic on $\mathbf{V} \times \mathbf{V}$, where the nonconforming space $\mathbf{V}$ is defined by $\mathbf{V} := \{\mathbf{v} \in \mathbf{H}^1_*(\Omega) \,|\, \int_\gamma [\mathbf{v}]\, ds = 0\}$, $\gamma := \partial\Omega_1 \cap \partial\Omega_2$. To see this, we set $\mathbf{v}|_{\Omega_1} := 0$ and $\mathbf{v}|_{\Omega_2} := \beta(x_2 - x_{2,c}, x_{1,c} - x_1)^T$, $\beta \neq 0$, where $(x_{1,c}, x_{2,c})^T$ denotes the center of gravity of γ. Then, $\mathbf{v} \in \mathbf{V}$ but $a(\mathbf{v},\mathbf{v}) = 0$.

Based on this observation, we define the nonconforming space

$$\mathbf{V}_{\mathbf{M}_H} := \left\{\mathbf{v} \in \mathbf{H}^1_*(\Omega) \,|\, \int_{\gamma_m} [\mathbf{v}] \cdot \boldsymbol{\mu}\, ds = 0,\, \boldsymbol{\mu} \in \mathbf{M}_H(\gamma_m),\, 1 \leq m \leq M\right\},$$

where $\mathbf{M}_H(\gamma_m) := (M_H(\gamma_m))^d$ is a suitable test space. If $\mathbf{M}_H(\gamma_m) \subset \mathbf{M}_h(\gamma_m)$ then $\mathbf{V}_h \subset \mathbf{V}_{\mathbf{M}_H}$, and for the uniform ellipticity on $\mathbf{V}_h \times \mathbf{V}_h$ it is sufficient to show the ellipticity on $\mathbf{V}_{\mathbf{M}_H} \times \mathbf{V}_{\mathbf{M}_H}$. A natural choice for $M_H(\gamma_m)$ is $P_1(\gamma_m)$. Unfortunately none of the considered Lagrange multiplier spaces satisfy $P_1(\gamma_m) \subset M_h(\gamma_m)$.

We introduce a new macro Lagrange multiplier space $M_H(\gamma_m)$ which has dimension two in 2D and dimension four in 3D. Let us start with the 2D case, and let $t \in [0,1]$ be a parametrization of the 1D interface γ_m, i.e., $x \in \overline{\gamma}_m$ if and only if $x = p_1 + t_x(p_2 - p_1)$, $t_x \in [0,1]$, where p_1 and p_2 are the two endpoints of γ_m. The ordering is arbitrary but fixed. Then, we decompose $\mathcal{P}_m$ into two disjoint subsets $\mathcal{P}^l_m := \{p \in \mathcal{P}_m \,|\, t_p \leq 0.5\}$ and $\mathcal{P}^r_m := \mathcal{P}_m \setminus \mathcal{P}^l_m$, and define

$$\mu_H := \Big(\frac{2}{t_l + t_r} - 1\Big) \sum_{p \in \mathcal{P}^l_m} \mu_p - \sum_{p \in \mathcal{P}^r_m} \mu_p\,,$$

where $t_l := \max\{t_p \,|\, p \in \mathcal{P}^l_m\} \leq 0.5$ and $t_r := \min\{t_p \,|\, p \in \mathcal{P}^r_m\} > 0.5$, see Figure 2.5. In the left, μ_H is given for the standard Lagrange multiplier space and in the right for the dual Lagrange multiplier space. It is easy to see that the mean value of μ_H is equal zero for the standard Lagrange multiplier space and the dual one based on piecewise linear functions. Now, we define

$$M_H(\gamma_m) := \operatorname{span}\{\varphi_H \in \Phi_H\}, \quad \Phi_H := \{1, \mu_H\},$$

in the 2D case, and in 3D, Φ_H is given as the corresponding product set. Thus for the 2D and 3D case, we have $M_H(\gamma_m) \subset M_h(\gamma_m)$.

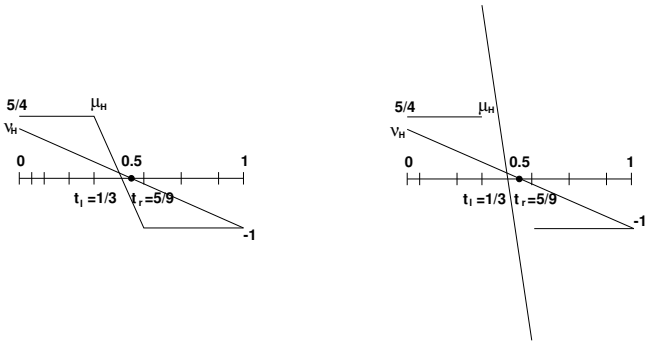

FIG. 2.5. *Test function μ_H and ν_H for standard (left) and dual (right) Lagrange multiplier space*

LEMMA 2.1. *Let $\mathbf{v} \in \mathbf{V}_{\mathbf{M}_H}$, and $\mathbf{v}$ restricted on Ω_k, $1 \le k \le K$, be a rigid body motion, then $\mathbf{v} = 0$.*

Proof. We start with a subdomain Ω_{k_0} such that $\partial\Omega_{k_0} \cap \Gamma_D$ has a non zero measure. Due to the Dirichlet boundary condition, $\mathbf{v}$ restricted to this subdomain is zero. Then, the interface condition yields that for all adjacent subdomains, we find in 2D

$$\int_{\gamma_m} \left(\mathbf{a} + \beta \begin{pmatrix} x_2 - x_{2,c} \\ x_{1,c} - x_1 \end{pmatrix} \right) \cdot \mathbf{e}_i \, ds = 0, \quad 1 \le i \le 2 \,,$$

where $\mathbf{e}_i$ denotes the i–th unit vector, and thus $\mathbf{a} = 0$. Introducing $\nu_H \in P_1(\gamma_m)$, $\nu_H(p_1) = -\nu_H(p_2) = 1$, see Figure 2.5, a straightforward computation shows that

$$\int_{\gamma_m} \mu_H \nu_H \, ds = \alpha_H |\gamma_m| \,,$$

where $\alpha_H \ge 1/3$ if $M_h(\gamma_m)$ is the piecewise linear dual Lagrange multiplier space as introduced in Subsection 2.1, and $\alpha_H \ge 2/9$ if $M_h(\gamma_m)$ is the standard Lagrange multiplier space and thus $\beta = 0$. We note that the lower bound for α_H does not depend on the mesh on γ_m. In 3D, the rigid body motions are given by $\mathbf{a} + \mathbf{b} \times (\mathbf{x} - \mathbf{x}_c)$, and similar arguments as in 2D yield $\mathbf{a} = \mathbf{b} = 0$. Starting from Ω_{k_0}, we can move to each other subdomain by crossing interfaces. □

LEMMA 2.2. *The bilinear form $a(\cdot,\cdot)$ is uniformly elliptic on $\mathbf{V}_H \times \mathbf{V}_H$.*

The lemma follows from the upper estimate for the broken H^1–norm

$$\|\mathbf{v}\|_1^2 \le C_1 a(\mathbf{v},\mathbf{v}) + C_2 \sum_{m=1}^{M} \sum_{\varphi_H \in \Phi_H} \| \int_{\gamma_m} \varphi_H [\mathbf{v}] \, ds \|^2, \quad \mathbf{v} \in \mathbf{H}^1_*(\Omega) \,, \tag{2.5}$$

where $\|\cdot\|$ stands for the Euclidean norm in $\mathbb{R}^d$. Inequality (2.5) is obtained by a Bramble–Hilbert argument and shown by contradiction. Here we do not work out the details but sketch the idea, for details we refer to [Woh99a]. We assume that (2.5) is not true. Then, the second Korn inequality and Lemma 2.1 give a contradiction. Although the space $\mathbf{V}_H$ depends on the triangulation, the ellipticity constant can be bounded from below independently of the triangulation.

REMARK 2.3. *Unfortunately, the proof by contradiction gives only the existence of such a constant C_1, but no information if C_1 can be chosen independently of the number of subdomains.*

It is likely that more elaborate techniques yield an ellipticity constant which is independent of the number of subdomains. For the scalar elliptic case in 2D, we refer to [Gop99] and for the three field approach to [BM00]. Both techniques are based on duality arguments and cannot be applied directly to our situation.

3. An equivalent formulation on the product space. In the previous section, we have given the saddle point formulation (2.3) on $\mathbf{X}_h \times \mathbf{M}_h$ and the positive definite nonconforming mortar formulation (2.4) on $\mathbf{V}_h$. Here, we reformulate the saddle point problem as a non–symmetric problem on the unconstrained product space $\mathbf{X}_h$ and eliminate the Lagrange multiplier $\boldsymbol{\lambda}_h$. Due to the biorthogonality (2.2), this can be done locally.

We start with the algebraic formulation of the saddle point problem. Let A_h and B_h be the matrices associated with the bilinear forms $a(\cdot,\cdot)$ on $\mathbf{X}_h \times \mathbf{X}_h$ and $b(\cdot,\cdot)$ on $\mathbf{X}_h \times \mathbf{M}_h$, respectively, and $\mathbf{f}_h$ the vector associated with the right hand side. The finite element solution $\mathbf{u}_h$ is decomposed into two components $\mathbf{u}_h^T = (\mathbf{u}_I^T, \mathbf{u}_N^T)$. We use the same symbol for an element in $\mathbf{X}_h$ and the corresponding vector in $\mathbb{R}^{n_h}$ with respect to the standard nodal basis, where n_h is the dimension of $\mathbf{X}_h$. All degrees of freedom associated with the interior vertices on the non–mortar sides are contained in the second component $\mathbf{u}_N$. The first component $\mathbf{u}_I$ includes all other degrees of freedom. We note that each degree of freedom is contained in exactly one of the two groups. By means of this decomposition, we can rewrite the saddle point problem (2.3) and find

$$\begin{pmatrix} A_h & B_h \\ B_h^T & 0 \end{pmatrix} \begin{pmatrix} \mathbf{u}_h \\ \boldsymbol{\lambda}_h \end{pmatrix} = \begin{pmatrix} A_{II} & A_{IN} & M \\ A_{NI} & A_{NN} & D \\ M^T & D & 0 \end{pmatrix} \begin{pmatrix} \mathbf{u}_I \\ \mathbf{u}_N \\ \boldsymbol{\lambda}_h \end{pmatrix} = \begin{pmatrix} \mathbf{f}_I \\ \mathbf{f}_N \\ 0 \end{pmatrix}, \tag{3.1}$$

where D is a diagonal matrix, and M is a sparse matrix with many zero blocks, and for each interface there is one rectangular mass matrix block, the band width of which depends on the local ratio of the meshsizes on mortar and adjacent non–mortar sides. The size of the diagonal matrix D is $d \cdot \sum_{m=1}^{M} \#\mathcal{P}_m$, and its entries are $\int_{\gamma_m} \phi_p \, ds$.

The second row of the saddle point problem (3.1) yields

$$\boldsymbol{\lambda}_h = D^{-1}(\mathbf{f}_N - A_{NI}\mathbf{u}_I - A_{NN}\mathbf{u}_N)\,. \tag{3.2}$$

We observe that for the standard Lagrange multiplier space D is not a diagonal matrix but a block mass matrix. Thus in that case, $\boldsymbol{\lambda}_h$ cannot be eliminated locally, and the inverse of a mass matrix enters. Introducing now $W_h^T := (0 \;\; D^{-1})$ and observing $B_h^T \mathbf{u}_h = 0$, we can rewrite $\boldsymbol{\lambda}_h$ in terms of W_h^T and the residual on the product space, $\boldsymbol{\lambda}_h = W_h^T(\mathbf{f}_h - A_h(\mathrm{Id} - W_h B_h^T)\mathbf{u}_h)$. Using this elimination in (3.1), we find

$$\begin{pmatrix} A_h & B_h \\ B_h^T & 0 \end{pmatrix} \begin{pmatrix} \mathrm{Id} \\ W_h^T A_h (W_h B_h^T - \mathrm{Id}) \end{pmatrix} \mathbf{u}_h = \begin{pmatrix} (\mathrm{Id} - B_h W_h^T)\mathbf{f}_h \\ 0 \end{pmatrix}. \tag{3.3}$$

In a last step, we reduce the number of equations by the dimension of $\mathbf{M}_h$. This can be done in different ways. We multiply (3.3) from the left by $(\mathbf{v}^T, \boldsymbol{\mu}^T)$ and set $\boldsymbol{\mu}$ as a function of $\mathbf{v}$. One possible choice is $\boldsymbol{\mu} := W_h^T A_h (W_h B_h^T - \mathrm{Id})\mathbf{v}$ yielding the symmetric system $A_{\mathrm{sym}}\mathbf{u}_h = \mathbf{f}_{\mathrm{sym}}$, where $\mathbf{f}_{\mathrm{sym}} := (\mathrm{Id} - B_h W_h^T)\mathbf{f}_h$ and

$$A_{\mathrm{sym}} := (\mathrm{Id}, (B_h W_h^T - \mathrm{Id}) A_h W_h) \begin{pmatrix} A_h & B_h \\ B_h^T & 0 \end{pmatrix} \begin{pmatrix} \mathrm{Id} \\ W_h^T A_h (W_h B_h^T - \mathrm{Id}) \end{pmatrix}. \tag{3.4}$$

A straightforward computation shows that $A_{\rm sym} = (B_h W_h^T - {\rm Id})A_h(W_h B_h^T - {\rm Id}) + B_h W_h^T A_h W_h B_h^T$. Considering the second block row of $A_{\rm sym}$ in more detail, we find $A_{NN}D^{-1}M^T\mathbf{u}_I + A_{NN}\mathbf{u}_N = 0$ or equivalently $W_h B_h^T \mathbf{u}_h = 0$. The choice $\boldsymbol{\mu} := W_h^T({\rm Id} - A_h)\mathbf{v}$ gives rise to the non–symmetric system

$$A_{\rm num}\mathbf{u}_h := ((B_h W_h^T - {\rm Id})A_h(W_h B_h^T - {\rm Id}) + W_h B_h^T)\mathbf{u}_h = \mathbf{f}_{\rm sym}\,. \tag{3.5}$$

In the rest of this section, we derive a variational problem for (3.5). We introduce a locally defined operator $P_h : \mathbf{X}_h \longrightarrow \mathbf{X}_h$ by

$$(P_h\mathbf{v})_i := \sum_{m=1}^{M}\sum_{p\in\mathcal{P}_m} \frac{\langle [v_i], \mu_p\rangle_{\gamma_m}}{\int\limits_{\gamma_m}\phi_p\,ds}\,\phi_p\,, \quad 1\le i\le d\,.$$

It is easy to see that the kernel of P_h is exactly the constrained space $\mathbf{V}_h$. The biorthogonality relation (2.2) yields that P_h is a projection. Furthermore, the algebraic representation of P_h is given by $W_h B_h^T$, and we find a new variational problem on the unconstrained product space. The algebraic system (3.5) can be written in terms of P_h as a variational problem: Find $\mathbf{u}_h \in \mathbf{X}_h$ such that

$$a(({\rm Id} - P_h)\mathbf{u}_h, ({\rm Id} - P_h)\mathbf{v}) + (P_h\mathbf{u}_h, \mathbf{v})_0 = f(({\rm Id} - P_h)\mathbf{v}), \quad \mathbf{v}\in\mathbf{X}_h\,. \tag{3.6}$$

LEMMA 3.1. *The variational problems (3.6) and (2.4) are equivalent.*

Proof. By definition, the solution of (2.4) is in the kernel of P_h, and thus is a solution of (3.6) by construction. Let $\mathbf{u}_h \in \mathbf{X}_h$ be a solution of (3.6). Then, it is sufficient to show that $P_h\mathbf{u}_h = 0$. We set $\mathbf{v} := P_h\mathbf{u}_h$ and find $(P_h\mathbf{u}_h, P_h\mathbf{u}_h)_0 = 0$. ∎

The unique solution $\mathbf{u}_h$ of (3.6) can be obtained by $\mathbf{u}_h = ({\rm Id} - P_h)\mathbf{w}_h$ from any solution $\mathbf{w}_h \in \mathbf{X}_h$ of

$$a(({\rm Id} - P_h)\mathbf{w}_h, ({\rm Id} - P_h)\mathbf{v}) = f(({\rm Id} - P_h)\mathbf{v}), \quad \mathbf{v}\in\mathbf{X}_h\,.$$

REMARK 3.2. *The new approach is based on the decomposition of $\mathbf{v}\in\mathbf{X}_h$ in $\mathbf{v} - P_h\mathbf{v}$ and $P_h\mathbf{v}$. Having the biorthogonality relation (2.2), the definition of P_h yields that $\mathbf{v} - P_h\mathbf{v} \in \mathbf{V}_h$. This is in general not true if we work with standard Lagrange multiplier spaces. In that case, P_h has to be replaced by a globally defined projection operator. Its application involves the inverse of a tridiagonal mass matrix in 2D and a band mass matrix in 3D.*

4. A modified multigrid method. In this section, we present our modified multigrid method. The implementation is based on the non–symmetric linear system (3.5) whereas the analysis of the convergence rates is done for the symmetric form (3.4). Let us assume that we have a nested sequence of global triangulations, and let us denote the associated unconstrained product spaces by $\mathbf{X}_l$, $0\le l\le L$. The meshsize is given by $h_l = 2h_{l+1}$, and the dimension of the space $\mathbf{X}_l$ is n_l. Working with standard nodal basis functions in $\mathbf{X}_l$ gives

$$ch_l^d\|\mathbf{v}_l\|^2 \le \|\mathbf{v}_l\|_0^2 \le Ch_l^d\|\mathbf{v}_l\|^2\,, \tag{4.1}$$

where $\|\cdot\|$ stands for the Euclidean vector norm of an element in $\mathbb{R}^{n_l}$. The Euclidean scalar product in $\mathbb{R}^{n_l}$ is denoted by $(\cdot,\cdot)$. In contrast to the constrained spaces $\mathbf{V}_l$, the product spaces $\mathbf{X}_l$ are nested. We denote the standard prolongation operator by $I_{l-1}^l : \mathbf{X}_{l-1} \longrightarrow \mathbf{X}_l$ and the restriction by $I_l^{l-1} : \mathbf{X}_l \longrightarrow \mathbf{X}_{l-1}$. For the rest of this section, we assume full H^2–regularity of the problem.

To obtain level independent convergence rates for our multigrid method, suitable approximation and smoothing properties have to be established. In a first step, we consider level dependent grid transfer operators $(I_{\mathrm{mod}})_l^{l-1}$ and $(I_{\mathrm{mod}})_{l-1}^{l}$ defined by

$$(I_{\mathrm{mod}})_l^{l-1} := (\mathrm{Id} - C_{l-1}^T) I_l^{l-1}, \quad (I_{\mathrm{mod}})_{l-1}^{l} := (\mathrm{Id} - C_l) I_{l-1}^{l}\,,$$

where $C_l := W_l B_l^T$. We observe that these transfer operators are obtained from the standard ones by a local post–processing step involving only the degrees of freedom on the interfaces but not the ones in the interior of the subdomains. It is easy to see that these transfer operators guarantee $C_{l-1}^T (I_{\mathrm{mod}})_l^{l-1} \mathbf{w}_l = 0$, $\mathbf{w}_l \in \mathbf{X}_l$, and $C_l (I_{\mathrm{mod}})_{l-1}^{l} \mathbf{w}_{l-1} = 0$, $\mathbf{w}_{l-1} \in \mathbf{X}_{l-1}$.

One basic tool to establish level independent convergence rates is a suitable approximation property. Here, we have to take into account the modified prolongation operator. Let $\mathbf{w}_l \in \mathbf{X}_l$ and $\mathbf{w}_{l-1} \in \mathbf{X}_{l-1}$ be the solutions of $A_{\mathrm{sym};l} \mathbf{w}_l = \mathbf{d}_l$ and $A_{\mathrm{sym};l-1} \mathbf{w}_{l-1} = \mathbf{d}_{l-1}$, respectively, where $\mathbf{d}_{l-1}$ is defined as the restriction of $\mathbf{d}_l$, i.e., $\mathbf{d}_{l-1} := (I_{\mathrm{mod}})_l^{l-1} \mathbf{d}_l$. The following lemma can be found for the scalar elliptic case in [WK01].

LEMMA 4.1. *Under the assumption that $C_l^T \mathbf{d}_l = 0$, we have the following approximation property*

$$\|\mathbf{w}_l - (I_{\mathrm{mod}})_{l-1}^{l} \mathbf{w}_{l-1}\| \leq C h_l^{2-d} \|\mathbf{d}_l\|\,.$$

Proof. Using the results from the previous section, observing that A_l is positive definite on $C_l \mathbf{X}_l$ and using the assumption on $\mathbf{d}_l$, we find $\mathbf{w}_l \in \mathbf{V}_l$ and $\mathbf{w}_{l-1} \in \mathbf{V}_{l-1}$. We define $\mathbf{f}_d \in \mathbf{X}_l \subset (L^2(\Omega))^d$ by $(\mathbf{f}_d, \mathbf{v}_l)_0 = (\mathbf{v}_l, \mathbf{d}_l)$, $\mathbf{v}_l \in \mathbf{X}_l$, and due to the norm equivalence (4.1), we obtain $h_l^d \|\mathbf{f}_d\|_0^2 \leq C \|\mathbf{d}_l\|^2$. Then, $\mathbf{w}_l$ and $\mathbf{w}_{l-1}$ are the mortar finite element approximations of $a(\mathbf{w}, \mathbf{v}) = (\mathbf{f}_d, \mathbf{v})_0$, $\mathbf{v} \in \mathbf{H}_*^1(\Omega)$, on level l and level $l-1$, respectively. By means of the H^2–regularity and the a priori estimate for the discretization error in the L^2–norm, we get

$$\|\mathbf{w}_l - \mathbf{w}_{l-1}\|_0 \leq C h_l^2 \|\mathbf{f}_d\|_0 \leq C h_l^{(2-d/2)} \|\mathbf{d}_l\|\,.$$

Then, the triangle inequality and the definition of the modified prolongation yield

$$\|\mathbf{w}_l - (I_{\mathrm{mod}})_{l-1}^{l} \mathbf{w}_{l-1}\| \leq \|\mathbf{w}_l - I_{l-1}^{l} \mathbf{w}_{l-1}\| + \|C_l I_{l-1}^{l} \mathbf{w}_{l-1}\|\,. \tag{4.2}$$

The first term is bounded by $C h_l^{-d/2} \|\mathbf{w}_l - \mathbf{w}_{l-1}\|_0 \leq C h_l^{2-d} \|\mathbf{d}_l\|$. To get an upper bound for the second term in (4.2), we have to consider the projection $P_l := P_{h_l}$ in more detail. Starting with the norm equivalence (4.1), we find

$$\|C_l I_{l-1}^{l} \mathbf{w}_{l-1}\|^2 \leq \frac{C}{h_l^d} \|P_l \mathbf{w}_{l-1}\|_0^2 \leq \frac{C}{h_l^{d-1}} \sum_{m=1}^{M} \|[\mathbf{w}_{l-1}]\|_{0;\gamma_m}^2\,.$$

In our last step, we use that the weighted L^2–norm of the jump at the interface of each element in $\mathbf{V}_{l-1}$, and thus for $\mathbf{w}_{l-1}$, can be bounded by a measure for its nonconformity, see [Woh99a]

$$\frac{1}{h_l} \sum_{m=1}^{M} \|[\mathbf{w}_{l-1}]\|_{0;\gamma_m}^2 \leq C \inf_{\mathbf{v} \in \mathbf{H}_*^1(\Omega)} \|\mathbf{v} - \mathbf{w}_{l-1}\|_1^2 \leq C\ h_l^2\ \|\mathbf{f}_d\|_0^2 \leq C h_l^{2-d} \|\mathbf{d}_l\|_0^2\,.$$

□

We note that for the proof of the approximation property, it is essential to have $\mathbf{w}_{l-1} \in \mathbf{V}_{l-1}$ and $\mathbf{w}_l \in \mathbf{V}_l$. In contrast to the standard Lagrange multiplier spaces, the dual basis Lagrange multiplier spaces are non–nested, i.e., $\mathbf{M}_{l-1} \not\subset \mathbf{M}_l$. The definition of the restriction $(I_{\mathrm{mod}})_l^{l-1}$ guarantees that $C_{l-1}^T \mathbf{d}_{l-1} = 0$ and thus $\mathbf{w}_{l-1} \in \mathbf{V}_{l-1}$. Within the multigrid algorithm, $\mathbf{d}_l$ is the defect after the presmoothing steps. To satisfy the assumption of Lemma 4.1, we have to guarantee that the iterate after the smoothing steps is in the constrained space $\mathbf{V}_l$. Starting with an arbitrary smoother for $\tilde{A}_l := (\mathrm{Id} - C_l^T) A_l (\mathrm{Id} - C_l)$, we construct a modified one satisfying this condition. We note that the matrix $(\tilde{A}_l)_{II}$ is symmetric and positive definite, the eigenvalues of which are bounded from below by ch_l^d and from above by Ch_l^{d-2}. Let $\tilde{G}_l$ be a smoother for $(\tilde{A}_l)_{II}$, e.g., a damped Jacobi method, extended trivially to the full space $\mathbf{X}_l$. We note that $\tilde{G}_l$ is singular on the full space $\mathbf{X}_l$, but the iterates $\tilde{\mathbf{y}}_l^i := \tilde{\mathbf{y}}_l^{i-1} + \tilde{G}_l(\mathbf{d}_l - \tilde{A}_l \tilde{\mathbf{y}}_l^{i-1})$, $i \geq 1$, are well defined. Then, we define our modified smoother by $G_l := (\mathrm{Id} - C_l)\tilde{G}_l(\mathrm{Id} - C_l^T)$, and denote the corresponding iterates by

$$\mathbf{y}_l^i := \mathbf{y}_l^{i-1} + G_l(\mathbf{d}_l - A_{\mathrm{sym};l}\, \mathbf{y}_l^{i-1}), \quad i \geq 1\,. \tag{4.3}$$

If $\mathbf{d}_l$ satisfies $C_l^T \mathbf{d}_l = 0$, then $\mathbf{d}_l$ is in the range of $\tilde{A}_l$. Let $\mathbf{w}_l$ be the solution of $A_{\mathrm{sym};l}\mathbf{w}_l = \mathbf{d}_l$, then $\tilde{\mathbf{w}}_l^T := ((\mathbf{w}_l)_I^T, (\tilde{\mathbf{y}}_l^0)_N^T)$ is a solution of $\tilde{A}_l \tilde{\mathbf{w}}_l = \mathbf{d}_l$, where $\tilde{\mathbf{y}}_l^0$ is the start iterate. The following lemma shows the relation between the two different iterates, $\mathbf{y}_l^i$ and $\tilde{\mathbf{y}}_l^i$, and we refer to [KW00a] for the scalar elliptic case.

LEMMA 4.2. *Under the assumptions $C_l^T \mathbf{d}_l = 0$ and $\mathbf{y}_l^0 = (\mathrm{Id} - C_l)\tilde{\mathbf{y}}_l^0$, the iterates $\mathbf{y}_l^i$ can be obtained from $\tilde{\mathbf{y}}_l^i$ by the local post–processing step*

$$\mathbf{y}_l^i = (\mathrm{Id} - C_l)\tilde{\mathbf{y}}_l^i\,, \qquad i \geq 1\,.$$

Moreover, the smoothing and stability properties of G_l are inherited from $\tilde{G}_l$, i.e.,

$$\|A_{\mathrm{sym};l}\mathbf{e}_l^i\| = \|\tilde{A}_l \tilde{\mathbf{e}}_l^i\|, \quad \|\mathbf{e}_l^i\| \leq C\|\tilde{\mathbf{e}}_l^i\|\,,$$

where $\mathbf{e}_l^i := \mathbf{w}_l - \mathbf{y}_l^i$ and $\tilde{\mathbf{e}}_l^i := \tilde{\mathbf{w}}_l - \tilde{\mathbf{y}}_l^i$ are the corresponding iteration errors.

Proof. Observing the special structure of the right hand side $\mathbf{d}_l$ and $\tilde{A}_l$, we obtain by induction

$$\begin{aligned} \mathbf{y}_l^{i+1} &= \mathbf{y}_l^i + (\mathrm{Id} - C_l)\tilde{G}_l(\mathrm{Id} - C_l^T)(\mathbf{d}_l - A_{\mathrm{sym};l}\, \mathbf{y}_l^i) \\ &= (\mathrm{Id} - C_l)(\tilde{\mathbf{y}}_l^i + \tilde{G}_l(\mathbf{d}_l - \tilde{A}_l \tilde{\mathbf{y}}_l^i)) \;\; = \;\; (\mathrm{Id} - C_l)\tilde{\mathbf{y}}_l^{i+1}\,, \end{aligned}$$

and thus $A_{\mathrm{sym};l}\mathbf{e}_l^i = \tilde{A}_l \tilde{\mathbf{e}}_l^i$. By means of $\mathbf{w}_l = (\mathrm{Id} - C_l)\mathbf{w}_l = (\mathrm{Id} - C_l)\tilde{\mathbf{w}}_l$, we find $\mathbf{e}_l^i = (\mathrm{Id} - C_l)\tilde{\mathbf{e}}_l^i$. Moreover, the norm of the scaled mass matrix $D_l^{-1}M_l^T$ is bounded independently of l. ∎

Now, our multigrid method for the solution of (3.4) will be defined in terms of the given modified transfer operators and the smoother G_l. The modified restriction operator and the zero start value for the defect correction guarantee that on each level $l < L$ the assumptions of Lemma 4.2 are satisfied. For $l = L$ the assumptions are satisfied by construction if we take zero or the prolongated solution on level $L-1$, i.e., $(I_{\mathrm{mod}})_{L-1}^L \mathbf{u}_{L-1}$, as start iterate. Then, we are in the setting of Lemma 4.2 for the presmoothing steps on all levels $l \leq L$. The same holds for the postsmoothing steps since we work with the modified prolongation. Furthermore, the smoother G_l yields that all iterates are in the kernel of C_l and thus the assumption of Lemma 4.1 is satisfied. Then, standard arguments give the main result of this section.

THEOREM 4.3. *The convergence rates for the $\mathcal{W}$–cycle are level independent provided that the number of smoothing steps is large enough.*

Proof. Approximation and smoothing properties yield level independent convergence rates, see, e.g., [Hac85, Th. 7.1.2]. ∎

We do not assemble the matrix $A_{\mathrm{sym};l}$. Working with $A_{\mathrm{num};l}$, we find that the iteration (4.3) can be replaced by

$$\mathbf{y}_l^i = \mathbf{y}_l^{i-1} + G_{\mathrm{num};l}(\mathbf{d}_l - A_{\mathrm{num};l}\,\mathbf{y}_l^{i-1})\,, \tag{4.4}$$

where $G_{\mathrm{num};l}$ is defined as an inexact block Gauß–Seidel smoother of $A_{\mathrm{num};l}$

$$A_{\mathrm{num};l} = \begin{pmatrix} (\tilde{A}_l)_{II} & 0 \\ D_l^{-1}M_l^T & \mathrm{Id} \end{pmatrix} \text{ and } G_{\mathrm{num};l} := \begin{pmatrix} (\tilde{G}_l)_{II} & 0 \\ -D_l^{-1}M_l^T(\tilde{G}_l)_{II} & \mathrm{Id} \end{pmatrix}.$$

A straightforward computation shows that (4.3) and (4.4) yield the same iterates. Furthermore, it is sufficient to work on the components of the index group I for the first $(m-1)$ smoothing steps. Here, m stands for the number of smoothing steps. Only in the last smoothing step, we have to apply (4.4) to both index groups N and I. This can be interpreted as one local post–processing step on the non–mortar side. Thus, the application of our multigrid method requires only a few additional multiplications with $D_l^{-1}M_l^T$, the complexity of which is of smaller order. It is equivalent to the multiplication of a scaled mass matrix associated with the $(d-1)$–dimensional interfaces.

REMARK 4.4. *The efficiency of the method is strongly connected to the use of dual basis functions. Working with standard Lagrange multiplier involves the inverse of a mass matrix instead of D_l^{-1}.*

5. Numerical results. In this section, we present numerical results illustrating the performance of our modified multigrid method. All our algorithms have been implemented within the framework of the finite element toolbox UG, see [BBJ+97]. In the first part of this section, we consider linear elasticity problems in 2D. A weak continuity condition at the interfaces is used in normal and tangential direction. In the second part, we present numerical results in 3D for scalar elliptic problems including an example with a geometrical nonconforming decomposition. In all examples, asymptotic constant convergence rates can be observed.

Figure 5.1 shows the deformation of a linear elastic body with inhomogeneous materials. Adaptive refinement techniques have been used in 2D. The refinement is controlled by a residual type error estimator for mortar finite elements, see [Woh99b, Woh99a]. The left picture in Figure 5.1 illustrates the problem setting. We apply two different surface pressures at the inhomogeneous Neumann boundary parts. The inhomogeneous Neumann boundary parts are marked by arrows in the left picture of Figure 5.1. Homogeneous Dirichlet boundary conditions are taken on the lower left corner of the domain, marked by Γ_D in the left picture of Figure 5.1. On the remaining boundary part, we apply homogeneous Neumann boundary conditions. The middle and right picture of Figure 5.1 shows the displacements of the solutions scaled by the factor ten and the final adaptive triangulations. In the middle picture, the applied Neumann boundary condition results in a constant displacement in normal direction at the corresponding boundary part. In the right picture, the applied Neumann boundary condition yields a linear displacement in normal direction at the corresponding boundary part. The deformation of the body in the neighborhood of the interfaces is in the right picture smaller than in the middle picture.

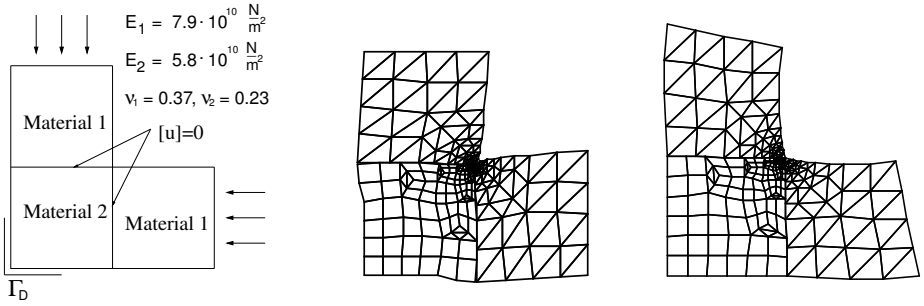

FIG. 5.1. *Coupling in normal and tangential direction in 2D, (Example 1)*

In our second example, we consider a nut–like geometry as depicted in Figure 5.2. The domain consists of 13 subdomains, and there are 6 inner crosspoints each of which has four adjacent subdomains. We choose silver as material with $\mu = 108280$ and $\lambda = 8517$. Inhomogeneous Dirichlet boundary conditions corresponding to a rotation by an angle of $\pi/500$ have been applied on the inner boundary Γ_I, i.e., the outer normal on Γ_I directs toward the center of gravity. We work with homogeneous boundary conditions on $\Gamma_O := \partial\Omega \setminus \Gamma_I$. On $\Gamma_O \cap \partial\Omega_k$ we take Neumann type boundary conditions if Ω_k is a triangle, and Dirichlet type boundary conditions if Ω_k is a square. Figure 5.2 shows the initial nonconforming triangulation, the displacements scaled by the factor 100 on the final triangulation, and the multigrid convergence rates of the $\mathcal{V}$–cycle and $\mathcal{W}$–cycle with three pre– and postsmoothing steps.

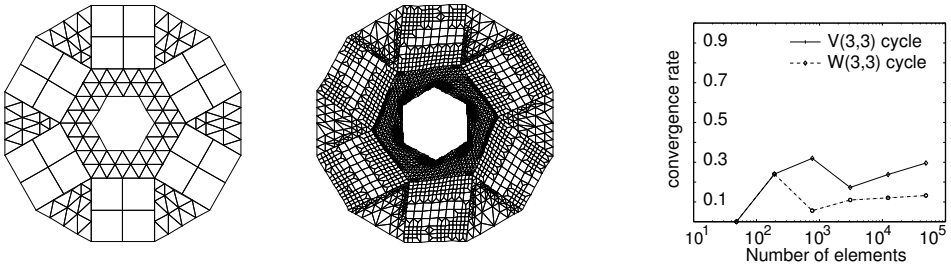

FIG. 5.2. *Initial triangulation (left), distorted grid (middle) and conv. rates (right), (Example 2)*

Examples 3 and 4 illustrate the convergence rate of our multigrid method in 3D, see [WK01]. Here, we use trilinear finite elements on hexahedrons and the piecewise linear dual Lagrange multiplier space introduced in Subsection 2.1. We compare the asymptotic convergence rates of the $\mathcal{V}$– and $\mathcal{W}$–cycles in case of one and three smoothing steps. The smoothing iteration is based on (4.4), and two different smoothers are compared. We define $(\tilde{G}_l)_{II}$ as a damped Jacobi method, i.e., $(\tilde{G}_l)_{II} := \omega(\mathrm{diag}((\tilde{A}_l)_{II}))^{-1}$, where $\omega = 0.7$, or as symmetric Gauß–Seidel smoother of $(\tilde{A}_l)_{II}$. Thus, one Gauß–Seidel step is roughly twice as expensive as one Jacobi step.

We consider a "Sandwich"–like domain build up of two different materials. The domain Ω is decomposed into three hexahedrons $\Omega_i := (0,1)^2 \times (z_i, z_{i+1})$, where $z_1 := 0, z_2 := 1, z_3 := 1.2, z_4 := 2.2$. The scalar elliptic model problem $-\mathrm{div}\, a\nabla u = 1$, on $\Omega := (0,1)^2 \times (z_1, z_4)$ is taken. Here, the coefficient a is piecewise constant,

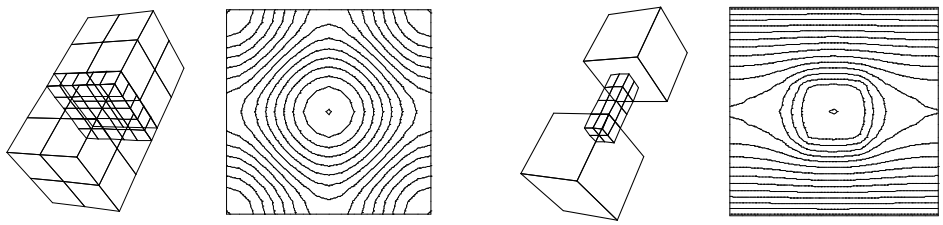

FIG. 5.3. *Initial triangulations and isolines for Example 3 (left) and Example 4 (right)*

$a|_{\Omega_i} := 100$, $i = 1, 3$ and $a|_{\Omega_2} := 1$. Dirichlet boundary conditions are applied on the upper and lower part of the domain, $u(x, y, z) = 1000\sqrt{(x - 1/2)^2 + (y - 1/2)^2} \cdot (1.0 - y/3) \exp(-10(x^2+y^2))$ if $z = z_1$ or $z = z_4$, and homogeneous Neumann boundary conditions elsewhere. In the left part of Figure 5.3, the nonmatching initial triangulation and the isolines at the interface are shown. The non–mortar sides are defined on the middle hexahedron. Figure 5.4 shows the convergence rates of Example 3 in 3D. In all cases, we observe level independent convergences rates. Even for the $\mathcal{V}(1,1)$–cycle, a constant asymptotic convergence rate is obtained.

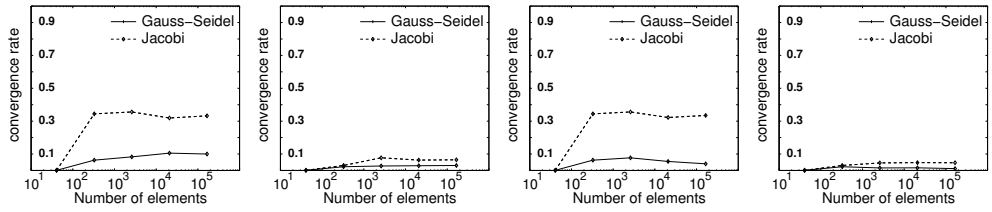

$\mathcal{V}(1,1)$–cycle $\mathcal{V}(3,3)$–cycle $\mathcal{W}(1,1)$–cycle $\mathcal{W}(3,3)$–cycle

FIG. 5.4. *Asymptotic conv. rates for Jacobi and symmetric Gauß–Seidel smoother (Example 3)*

In Example 4, we consider the domain depicted in the right part of Figure 5.3. It is decomposed into three subdomains $\Omega_1 := (0,1)^2 \times (z_1, z_2)$, $\Omega_2 := (1/3, 2/3)^2 \times (z_2, z_3)$, $\Omega_3 := (0,1)^2 \times (z_3, z_4)$ where $z_1 := 0$, $z_2 := 1$, $z_3 = 2$, $z_4 = 3$. We remark that we are in the geometrical nonconforming situation. In particular, the non–mortar sides on Ω_2 cover only a part of the adjacent mortar sides on Ω_1 and Ω_3. We impose Dirichlet boundary values on parts of $\partial\Omega_1$ and $\partial\Omega_3$, and set $u(x, y, z) = 10$ for $\{(x, y, z) \in \partial\Omega_1 \,|\, z = z_1\}$ and $\{(x, y, z) \in \partial\Omega_3 \,|\, z = z_4\}$, elsewhere we impose homogeneous Neumann boundary conditions, see [WK01].

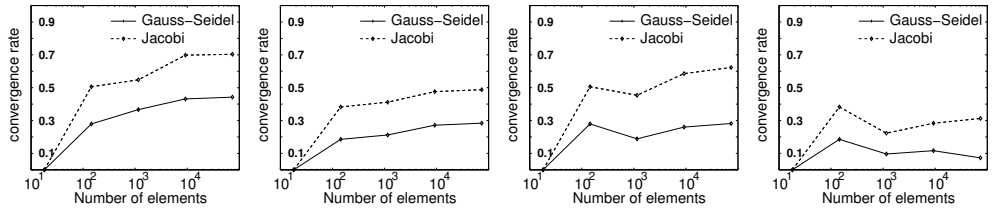

$\mathcal{V}(1,1)$–cycle $\mathcal{V}(3,3)$–cycle $\mathcal{W}(1,1)$–cycle $\mathcal{W}(3,3)$–cycle

FIG. 5.5. *Asymptotic conv. rates for Jacobi and symmetric Gauß–Seidel smoother (Example 4)*

The numerical results are shown in Figure 5.5. The performance is not as good

as in Example 3, but the asymptotic convergence rates seem to be independent of the refinement level. Increasing the number of smoothing steps yields considerably better results. In both examples, the Gauß–Seidel smoother has better convergence rates than the Jacobi type smoother. The performance of the Gauß–Seidel smoother is in Example 4 better than for the Jacobi smoother. Three Jacobi steps are required to obtain approximately the same convergence rates as for one symmetric Gauß–Seidel step.

6. Free displacement in tangential direction. In this section, we introduce the necessary modifications of our method if the coupling condition is enforced only in normal direction. Since the direction of the outer normal cannot be assumed to be constant along the interfaces, we have to introduce some suitable local coordinate transformations, see [Woh99a]. These transformations have the character of a rotation of the local coordinate system.

We define the bilinear form $b_n(\cdot,\cdot)$ corresponding to the coupling in normal direction at the interface by

$$b_n(\mathbf{v},\mu) := \sum_{m=1}^{M} \langle [\mathbf{v}\cdot\mathbf{n}], \mu\rangle_{\gamma_m} , \qquad \mu \in M_h := \prod_{m=1}^{M} M_h(\gamma_m) ,$$

where $\mathbf{n}$ is the outer normal of the subdomain on the non–mortar side. Now, we replace the bilinear form $b(\cdot,\cdot)$ in (2.3) by the modified one and obtain the following saddle point problem: Find $(\mathbf{u}_h^n, \lambda_h) \in \mathbf{X}_h \times M_h$ such that

$$\begin{aligned} a(\mathbf{u}_h^n, \mathbf{v}) + b_n(\mathbf{v}, \lambda_h) &= f(\mathbf{v}), \qquad \mathbf{v} \in \mathbf{X}_h , \\ b_n(\mathbf{u}_h^n, \mu) &= 0, \qquad \mu \in M_h . \end{aligned} \tag{6.1}$$

At first glance, it has the same structure as (2.3). However, there is an essential difference. The new bilinear form $b_n(\cdot,\cdot)$ is defined on $\mathbf{X}_h \times M_h$, where M_h is, in contrast to $\mathbf{M}_h$, a scalar space. Using the same decomposition as before, i.e., $(\mathbf{u}_h^n)^T = ((\mathbf{u}_I^n)^T, (\mathbf{u}_N^n)^T)$, we find for the algebraic representation of (6.1)

$$\begin{pmatrix} A_{II} & A_{IN} & M_n \\ A_{NI} & A_{NN} & D_n \\ M_n^T & D_n^T & 0 \end{pmatrix} \begin{pmatrix} \mathbf{u}_I^n \\ \mathbf{u}_N^n \\ \lambda_h \end{pmatrix} = \begin{pmatrix} \mathbf{f}_I \\ \mathbf{f}_N \\ 0 \end{pmatrix} . \tag{6.2}$$

In contrast to D in (3.1), D_n is not a diagonal matrix but a $d\,n_h \times n_h$ block diagonal matrix, where n_h is the dimension of M_h. Each block is associated with an interior vertex on the non–mortar side, and the block size is given by $d \times 1$. Thus, we cannot eliminate the Lagrange multiplier as easy as in (3.2). Let $\mathcal{P} := \cup_{m=1}^{M} \mathcal{P}_m$ be the set of interior vertices on the non–mortar sides. Then, we can write D_n as $D_n := \mathrm{diag}(\mathbf{d}_p)_{p\in\mathcal{P}}$, where $\mathbf{d}_p \in \mathbb{R}^d$ is defined by

$$\mathbf{d}_p := \frac{1}{2^{d-1}} \sum_{e\in\Sigma_p} |e| \;\; \mathbf{n}_e .$$

Here, Σ_p is the set of elements, i.e., edges in 2D or faces in 3D, on the non–mortar side sharing the vertex p, and $\mathbf{n}_e$ is the constant outer unit normal vector on the element e. We assume that $\mathbf{d}_p \neq 0$. Starting with $\mathbf{b}_1 := \mathbf{d}_p/\|\mathbf{d}_p\|$, we introduce for each vertex $p \in \mathcal{P}$ an orthonormal basis $\mathcal{B} := \{\mathbf{b}_1, \ldots, \mathbf{b}_d\}$ in $\mathbb{R}^d$. The orthogonal transformation which maps $\mathcal{B}$ to the canonical basis of $\mathbb{R}^d$ is denoted by $\mathcal{O}_p \in \mathbb{R}^{d\times d}$.

An explicit representation of $\mathcal{O}_p$ can be obtained, e.g., as Householder transformation. For $\mathbf{v} \in \mathbf{X}_h$, we denote by $\mathbf{v}_p \in \mathbb{R}^d$ the degrees of freedom associated with the vertex p. We define $\mathcal{O}_p \mathbf{v}_p =: (w_n, \mathbf{w}_T^T)^T$ and call w_n and $\mathbf{w}_T$ the normal and tangential component of $\mathbf{v}$ at the vertex p, respectively. Then, we define the global orthonormal transformation $\mathcal{O}_N$ by

$$\mathcal{O}_N := \operatorname{diag}(\mathcal{O}_p)_{p \in \mathcal{P}} .$$

We apply the coordinate transformation represented by $\operatorname{diag}(\mathrm{Id}, \mathcal{O}_N, \mathrm{Id})$ to (6.2) and find the symmetric system

$$\begin{pmatrix} A_{II} & A_{IN}\mathcal{O}_N^T & M_n \\ \mathcal{O}_N A_{NI} & \mathcal{O}_N A_{NN}\mathcal{O}_N^T & \mathcal{O}_N D_n \\ M_n^T & D_n^T \mathcal{O}_N^T & 0 \end{pmatrix} \begin{pmatrix} \mathbf{u}_I^n \\ \mathcal{O}_N \mathbf{u}_N^n \\ \lambda_h \end{pmatrix} = \begin{pmatrix} \mathbf{f}_I \\ \mathcal{O}_N \mathbf{f}_N \\ 0 \end{pmatrix} . \tag{6.3}$$

Due to the construction of $\mathcal{O}_N$, we have $\mathcal{O}_N^T \mathcal{O}_N = \mathrm{Id}$ and $\mathcal{O}_p \mathbf{d}_p = (\|\mathbf{d}_p\|, \mathbf{0})^T$. Observing that $D_n^T D_n$ is a diagonal matrix, the entries of which are given by $\|\mathbf{d}_p\|^2$, the Lagrange multiplier λ_h can be locally eliminated by

$$\lambda_h = (D_n^T D_n)^{-1} D_n^T (\mathbf{f}_N - A_{NI}\mathbf{u}_I - A_{NN}\mathbf{u}_N) .$$

In our last step, we can rearrange the indices. The new index group I includes now the former index group I plus the tangential components of the vectors in the former index group N. The new index group N is a subset of the former index group N and contains the normal components. We observe, that the submatrix of $\mathcal{O}_N D_n$ corresponding to the new index group N is diagonal. Thus, we can proceed as in Section 3. Using this new index grouping, we get exactly the same structure of the saddle point problem as in (3.1), and the proposed multigrid algorithm can be applied on (6.3).

Finally, we show some numerical results, illustrating the difference between the two coupling conditions at the interfaces. We start with the 2D example of Section 5 and consider two different boundary conditions. In the first situation, see the middle picture of Figure 6.1, we use a constant displacement in normal direction at the upper and right boundary part of the domain. The second situation is defined by a linear displacement in normal direction at the upper and right boundary part of the domain. As in Section 5, the lower left corner of the domain is fixed, i.e., we apply homogeneous Dirichlet boundary conditions on Γ_D. Compared to Section 5, we use a weaker coupling condition at the interfaces. Here, the bodies are not glued together, and free tangential displacement is permitted. The coupling condition in normal direction can be viewed as a kind of non penetration condition of the bodies with respect to the reference configuration.

Figure 6.1 displays the displacement of the solution scaled by the factor 10. Due to the tangential displacement, penetration might be observed at the interface, see the right picture in Figure 6.1. Although, the proposed algorithm does not solve a nonlinear contact problem, we can use the method as an inner iteration scheme within an outer scheme used to detect the actual zone of contact. Once the actual contact boundary is known, our algorithm solves the contact problem, and no penetration occurs. The drawback of this method is that in each outer iteration step a mass matrix has to be assembled.

Figure 6.2 shows a model problem in 3D. The displacement of the solution and the coarse triangulation are given for the saddle point problems (2.3) and (6.1). On

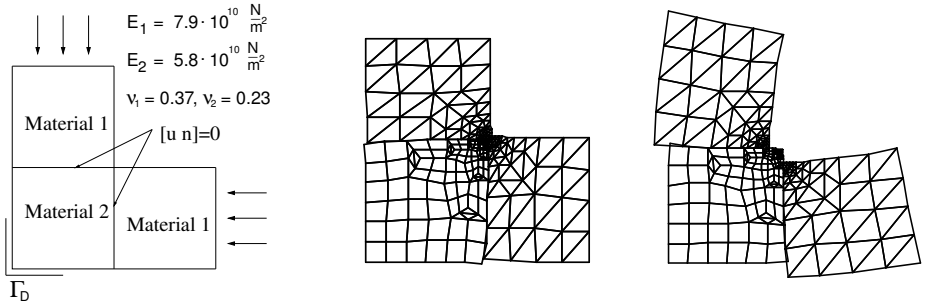

FIG. 6.1. *Coupling in normal direction and free tangential displacement in 2D*

the left, the Lagrange multiplier space has three degrees of freedom per node, one degree in each direction. The mortar finite element solution satisfies a weak continuity condition in tangential and normal direction. In the second situation on the right of Figure 6.2, there is no continuity condition for the tangential displacement. Thus, we replace the bilinear form $b(\cdot,\cdot)$ in the saddle point formulation by $b_n(\cdot,\cdot)$, and work with the modifications proposed in this section.

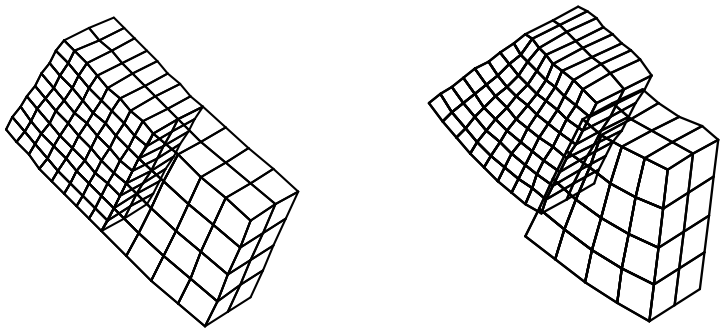

FIG. 6.2. *Coupling in both directions (left) and in normal direction (right) in 3D*

Figure 6.2 shows the structural difference between the two weak coupling conditions at the interface. On the left, there is no relative displacement of the two bodies in tangential direction, whereas in the situation on the right, a sliding between the two bodies is permitted. A relative displacement of the left body with respect to the right body can be observed. We remark that the nonconforming space $\mathbf{V}_h$ is a subspace of the kernel $\mathbf{V}_h^n$ of $(B_h^n)^T$ associated with the bilinear form $b_n(\cdot,\cdot)$. In the general situation that $\partial\Omega_k \cap \Gamma_D$ is empty for some subdomain indices, the ellipticity of $a(\cdot,\cdot)$ on $\mathbf{V}_h^n \times \mathbf{V}_h^n$ is lost, and rigid body motions are contained in $\mathbf{V}_h^n$. We obtain unique solvability in our example by imposing Dirichlet boundary conditions on one face of each subdomain.

7. Elastic contact of two bodies. In this section, we consider a new algorithm for the elastic contact between deformable bodies. The numerical simulation of elastic contact has been extensively studied in various papers, see, e.g., [DNS99, WG97, HH80, HH81, ESW99]. For a survey, we refer to [Wri95, IHL88, KO88] and the references therein. One of the major difficulties in the numerical simulation of contact problems is the non–differentiability of the associated energy functional at the contact

boundary. Regularization techniques (penalty methods) are widely used, see, e.g., [CSW99, ESW99], as well as augmented Lagrangian methods [Tal94, PC99]. Here, we combine monotone multigrid methods [Kor97a, KK99] with mortar techniques. The information transfer at the contact boundary is realized in terms of the scaled mass arising from the mortar method with dual Lagrange multipliers.

For simplicity, we restrict ourselves to the case of two deformable bodies in contact, see Figure 7.1. The two bodies in their reference configuration are identified with the domains Ω_k, $k = 1, 2$, and we decompose the solution $\mathbf{u}$ in $\mathbf{u} = (\mathbf{u}_1, \mathbf{u}_2)$, and write $(\mathbf{u}_k)_n := \mathbf{u}_k \cdot \mathbf{n}_k$, $k = 1, 2$, where $\mathbf{n}_k$ is the outer unit normal on $\partial\Omega_k$. Let us now formulate the contact problem between two linear elastic bodies as boundary value problem. We decompose the boundary of Ω in three disjoint parts, Γ_D is the Dirichlet part, Γ_F denotes the Neumann part and Γ_C stands for the contact boundary. We note that the actual contact zone between the two bodies unknown in advance, and it is assumed to be a subset of Γ_C. In addition to the equilibrium conditions in Ω and boundary conditions on $\partial\Omega$

$$\begin{array}{rcll} -\sigma_{ij}(\mathbf{u})_{,j} & = & f_i, & \text{in } \Omega\,, \\ \mathbf{u} & = & 0, & \text{on } \Gamma_D\,, \\ \sigma_{ij}(\mathbf{u}) \cdot n_j & = & p_i, & \text{on } \Gamma_F\,, \end{array} \tag{7.1}$$

we have the following conditions on the possible contact boundary Γ_C

$$\begin{array}{rcccl} \sigma_T(\mathbf{u}_1) & = & \sigma_T(\mathbf{u}_2) & = & 0\,, \\ \sigma_n(\mathbf{u}_1) & = & \sigma_n(\mathbf{u}_2) & \leq & 0\,, \end{array} \tag{7.2}$$

and the linearized contact condition on Γ_C

$$\begin{array}{rcl} t & \geq & (\mathbf{u}_1)_n + (\mathbf{u}_2)_n\,, \\ 0 & = & ((\mathbf{u}_1)_n + (\mathbf{u}_2)_n - t)\,\sigma_n(\mathbf{u}_1)\,, \end{array} \tag{7.3}$$

where the function $t\colon \Gamma_C \subset \mathbb{R}^d \longrightarrow \mathbb{R}$ is the distance between the two bodies in normal direction taken with respect to the reference configuration. Here, we consider a contact problem without friction. Thus, the tangential component of the stress tensor vanishes at the contact boundary, and is set to zero in the first equation of (7.2). We have only contact pressure at Γ_C. If there is no contact between the two bodies, the boundary stresses at Γ_C are zero, see Equations (7.2) and (7.3). For details of the problem formulation, we refer to [HH80, BGK87]. We write $f(\mathbf{v}) := (\mathbf{v}, \mathbf{f})_{0;\Omega} + (\mathbf{v}, \mathbf{p})_{0;\Gamma_F}$ and denote by $f_k(\cdot)$ and $a_k(\cdot,\cdot)$ the restriction of $f(\cdot)$ and $a(\cdot,\cdot)$ to Ω_k, $k = 1, 2$, respectively. In general, the zone of actual contact is unknown, and thus the contact problem is nonlinear and non–differentiable with respect to the displacements at the contact boundary. The corresponding weak formulation results in a variational inequality. Let us define the convex set $\mathcal{K}$ of admissible displacements by

$$\mathcal{K} = \{\mathbf{v} \in \mathbf{H}^1_*(\Omega_1) \times \mathbf{H}^1_*(\Omega_2) \mid (\mathbf{v}_1)_n + (\mathbf{v}_2)_n \leq t\}\,.$$

The weak form of (7.1)–(7.3) is given by a variational inequality: Find $\mathbf{u} \in \mathcal{K}$ such that

$$a(\mathbf{u}, \mathbf{v} - \mathbf{u}) \geq f(\mathbf{v} - \mathbf{u}), \qquad \mathbf{v} \in \mathcal{K}\,,$$

which is equivalent to minimizing the energy functional $J(\mathbf{v}) := \frac{1}{2}a(\mathbf{v}, \mathbf{v}) - f(\mathbf{v})$ on $\mathcal{K}$, see, e.g., [HH80, BGK87].

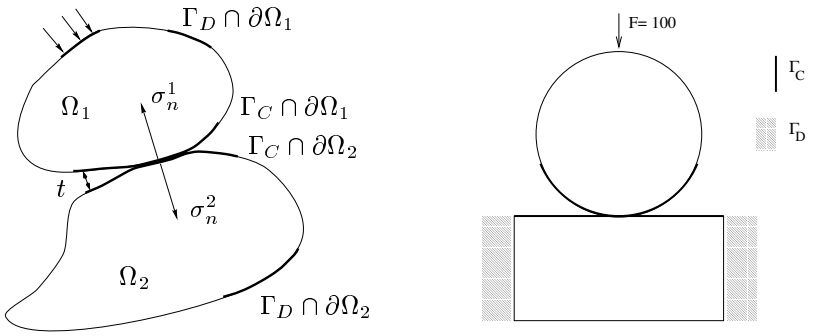

FIG. 7.1. *Two elastic bodies in contact (left) and Hertzian contact problem (right)*

Our approach is based on a Dirichlet–Neumann algorithm with inexact solvers. In each step, a nonlinear one–sided contact problem has to be solved. This is done on the discrete level by a monotone multigrid method, see [Kor97b, KK00]. Furthermore, an inhomogeneous Neumann problem has to be solved. Here, we apply standard multigrid techniques. The information transfer at the contact boundary will be realized in terms of dual mortar methods. The major advantages of this new approach are the efficiency of the iterative solver, and the a priori estimates for the boundary stresses at the actual contact zone. In contrast to penalty methods, the discretization error of the boundary stresses does not depend on regularization parameters.

To motivate our approach, let us assume for the moment that the contact stress σ_n is known on Γ_C. Then, problem (7.1)–(7.3) can be decoupled in the following way: In a first step, we solve an inhomogeneous Neumann problem on Ω_2: Find $\mathbf{u}_2 \in \mathbf{H}^1_*(\Omega_2)$ such that

$$a_2(\mathbf{u}_2, \mathbf{v}) = f_2(\mathbf{v}) + (\sigma_n, \mathbf{v}_n)_{0;\Gamma_C}, \qquad \mathbf{v} \in \mathbf{H}^1_*(\Omega_2)\,.$$

Having $\mathbf{u}_2 \in \mathbf{H}^1_*(\Omega_2)$, $\mathbf{u}_1 \in \mathbf{H}^1_*(\Omega_1)$ can be obtained in terms of $\mathbf{u}_2|_{\Gamma_C}$ as the solution of a one–sided contact problem. We define the convex set $\mathcal{K}_g$ of admissible displacements for the scalar function g by

$$\mathcal{K}_g := \{\mathbf{v}_1 \in \mathbf{H}^1_*(\Omega_1) \mid (\mathbf{v}_1)_n \le t - g \text{ on } \Gamma_C\}\,.$$

Then, the one–sided contact problem can be written as a variational inequality: Find $\mathbf{u}_1 \in \mathcal{K}_{(\mathbf{u}_2)_n}$ such that

$$a_1(\mathbf{u}_1, \mathbf{v} - \mathbf{u}_1) \;\ge\; f_1(\mathbf{v} - \mathbf{u}_1), \qquad \mathbf{v} \in \mathcal{K}_{(\mathbf{u}_2)_n}\,. \tag{7.4}$$

The discretization of the set $\mathcal{K}_g$ is given by

$$\mathcal{K}_g^h := \{\mathbf{v}_1 \in \mathbf{X}_{1,h} \mid (\mathbf{v}_1)_n(p) \le t(p) - g(p) \text{ for all } p \in \mathcal{T}_{h_1} \cap \Gamma_C\}\,, \tag{7.5}$$

where $\mathbf{X}_{k,h}$ is the finite element space $\mathbf{X}_h \cap \mathbf{H}^1_*(\Omega_k)$, $k = 1, 2$. Here, we assume that g and t are continuous. Then, a priori estimates for the discretization error can be found in, e.g., [KO88]. In the following, we also denote the discrete approximation by $\mathbf{u} = (\mathbf{u}_1, \mathbf{u}_2) \in \mathbf{X}_{1,h} \times \mathbf{X}_{2,h}$, and we do not use an additional index h, and $\boldsymbol{\lambda} \in \mathbf{M}_h$ stands for the discrete boundary stress.

The variational inequality (7.4) can be solved efficiently by monotone multigrid methods. Here, the main idea is to minimize the energy functional $J_1(\cdot)$ on $\mathcal{K}^h_{(\mathbf{u}_2)_n}$

successively in direction of appropriate test functions. Choosing the multilevel nodal basis of a multigrid hierarchy as test functions, this turns out to be a combination of a projected block Gauß–Seidel on the finest grid with locally damped coarse grid corrections, and can be implemented as a modified $\mathcal{V}$–cycle. Since the coarse grid corrections have to satisfy the constraints given by (7.5) with respect to the finest triangulation, suitable non–trivial coarse grid functions have to be constructed. It can be shown, that after a finite number of iterations the discrete contact boundary is identified. Then, the method degenerates to a standard multigrid method with special treatment of the eventually curvilinear contact boundary. For details, we refer to [Kor97a, KK99, KK00]. Moreover in the mortar setting, the Lagrange multiplier plays the role of Neumann boundary conditions. In the dual approach, the contact stress σ_n can be obtained from the residual by a local post–processing step. The combination of mortar finite elements, monotone multigrid methods and domain decomposition techniques defines in a natural way a new solution algorithm for elastic contact problems. It can be interpreted as a Dirichlet–Neumann type algorithm. We define the mortar side to be on the contact boundary of Ω_2, and the non–mortar side is the adjacent side on the contact boundary of Ω_1. Let us introduce the transfer operator $S_h\colon \mathbf{X}_{2,h} \longrightarrow \mathbf{X}_{1,h}$,

$$(S_h \mathbf{v})_i := \sum_{p \in \mathcal{P}} \frac{\langle v_i, \mu_p \rangle_{\Gamma_C}}{\int\limits_{\Gamma_C} \phi_p \, ds} \, \phi_p \,, \quad \mathbf{v} \in \mathbf{X}_{2,h} \,, \quad 1 \le i \le d \,,$$

where ϕ_p is the scalar nodal basis function in Ω_1 associated with the vertex p, and $\mathcal{P}$ is the set of vertices on the non–mortar side of $\overline{\Gamma}_C$. In contrast to the previous sections, the vertices on the boundary of Γ_C are included, and no modification of the dual basis function μ_p is necessary in the neighborhood of the boundary of Γ_C. Denoting the matrix representation of S_h by S, we observe that S is a $n_1 \times n_2$ matrix, $n_k := \dim \mathbf{X}_{k,h}$, $k = 1, 2$, which consists of large zero blocks and one non zero block associated with the vertices on the non–mortar and mortar side.

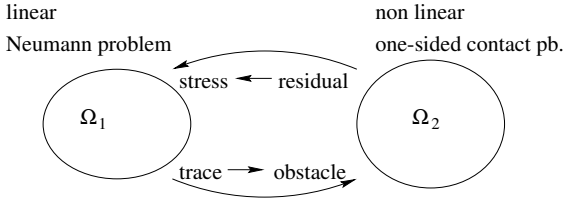

FIG. 7.2. *Nonlinear Dirichlet–Neumann type algorithm*

Before we present our nonlinear Dirichlet–Neumann algorithm which is illustrated in Figure 7.2, we introduce some notation. For $k = 1, 2$, we denote by A_k the stiffness matrix with respect to $a_k(\cdot, \cdot)$ and by $\mathbf{f}_k$ the vector associated with the right hand side, i.e., $f_k(\mathbf{v}) = (\mathbf{f}_k, \mathbf{v})$, $\mathbf{v} \in \mathbf{X}_{k,h}$. Using the same techniques as in Section 6, we define for each $\mathbf{g} \in \mathbf{X}_h$ by means of the local rotations $\mathcal{O}_p$ a continuous function $g_n\colon \Gamma_C \longrightarrow \mathbb{R}$. Here, in an abuse of notation, we do not distinguish between an element $\mathbf{v} \in \mathbf{X}_h$ and its vector representation with respect to the standard nodal basis. In addition, we identify the spaces $\mathbf{X}_{k,h}$ and $\mathbb{R}^{n_k}$, $k = 1, 2$. Now, our Dirichlet–Neumann algorithm in its algebraic formulation is defined as follows:

Choose damping parameters: $0 < \eta_1, \eta_2 \leq 1$.
Initialize: $\mathbf{X}_{1,h} \ni \mathbf{g}^{-1} = 0,\ \mathbf{X}_{2,h} \ni \mathbf{p}^0 = 0$.
For $\mu = 0, \ldots, N$ *do*

Solve linear Neumann problem: Find $\mathbf{u}_2^\mu \in \mathbf{X}_{2,h}$*:*

$$A_2 \mathbf{u}_2^\mu = \mathbf{f}_2 + \mathbf{p}^\mu \,.$$

Transfer of displacements and damping:

$$\mathbf{g}^\mu = (1-\eta_1)\mathbf{g}^{\mu-1} + \eta_1 S \mathbf{u}_2^\mu \,.$$

Solve nonlinear one–sided contact problem: Find $\mathbf{u}_1^\mu \in \mathcal{K}^h_{g_n^\mu}$*:*

$$(A_1 \mathbf{u}_1^\mu, \mathbf{v} - \mathbf{u}_1^\mu) \geq (\mathbf{f}_1, \mathbf{v} - \mathbf{u}_1^\mu), \qquad \mathbf{v} \in \mathcal{K}^h_{g_n^\mu} \,.$$

Compute the linear residual $\mathbf{r}_1^\mu \in \mathbf{X}_{1,h}$*:*

$$\mathbf{r}_1^\mu = A_1 \mathbf{u}_1^\mu - \mathbf{f}_1 \,.$$

Transfer of scaled boundary stresses and damping:

$$\mathbf{p}^{\mu+1} = (1-\eta_2)\mathbf{p}^\mu + \eta_2 S^T \mathbf{r}_1^\mu \,.$$

The transfer of the Dirichlet values at the contact boundary is realized in terms of the operator S_h and the transfer of the scaled boundary stresses in terms of the adjoint operator S_h^*, corresponding to the duality between displacements and stresses. In the algebraic formulation, the matrix S is used to transfer the displacements on the mortar side as Dirichlet values, or more precisely as an obstacle, onto the non–mortar side, and the scaled boundary stresses are transferred from the non–mortar side onto the mortar side in terms of the transposed matrix S^T. The interface conditions of the mortar formulation guarantee that (7.2) and (7.3) are satisfied in a weak integral form. For frictionless contact, the first equation in (7.2) can also be satisfied in its strong form. Then, the Lagrange multiplier space is a scalar function and the mortar approach has to be modified according to Section 6. Here, we work with the more general approach that the Lagrange multiplier space is also vector valued.

REMARK 7.1. *Using the vector valued approach for the Lagrange multiplier space, friction terms can be easily included. The first equation in (7.2) has to be replaced by some friction law, e.g., the Coulomb friction.*

Let us now consider the matrix S in more detail. Setting $D_S = \mathrm{diag}(\mathbf{d}_p)_{p\in\mathcal{P}}$ and $\mathbf{d}_p \in \mathbb{R}^{d\times d} = \mathrm{diag}(\int_{\Gamma_C} \phi_p \, ds)_{1\leq i\leq d}$, we can write the non zero block of S as a scaled mass matrix $D_S^{-1} M_S^T$. Here, the mass matrix M_S corresponds to the duality pairing $\langle \cdot, \cdot \rangle_{\Gamma_C}$. Then, $D_S^{-1} M_S^T$ is closely related to the scaled mass matrix matrix $D^{-1} M^T$ given in Section 3. The entries of M_S are given by $\int_{\Gamma_C} \phi_{p'} \, \mu_p \, ds$, where $\phi_{p'}$ is the scalar nodal basis function in Ω_2 associated with the vertex $p' \in \Gamma_C$. Due to the jump $[\cdot]$ in the definition of the bilinear form $b(\cdot,\cdot)$, the entries of M have the opposite sign. Considering implementational aspects, we observe that the same subfunctions can be used for assembling M and M_S. Moreover for a suitable index ordering, we find

$$S = \begin{pmatrix} D_S^{-1} M_S^T & 0 \\ 0 & 0 \end{pmatrix} ,$$

and the application of the operator S_h requires only the multiplication with a scaled mass matrix on the contact boundary.

Furthermore, the boundary stress $\boldsymbol{\lambda}$ can be obtained by a local post–processing step from the final residual $\mathbf{r}_1^N$,

$$\boldsymbol{\lambda} \;=\; (D_S^{-1} \;\; 0)\, \mathbf{r}_1^N \,.$$

In a last step, we get the normal stress σ_n and the tangential stress σ_T by a local rotation from $\boldsymbol{\lambda}$. We remark, that the numerical results show that $\sigma_T = 0$, although we do not enforce this condition.

REMARK 7.2. *If the actual contact zone is known, problem (7.1)–(7.3) will be linear. In this case, we can expect the same order of convergence as for a standard Dirichlet–Neumann type preconditioner.*

Finally, we present numerical examples for the proposed algorithm. Our first test problem is the Hertzian contact of a linear elastic circle with a linear elastic plane. In this example, the contact stresses can be computed analytically [Her82]. To test the performance of our algorithm, we compare the computed boundary stresses with the analytical ones. For comparability, we choose the same problem data and geometry as in [CSW99]. We consider an elastic circle with scaled material parameters $E = 7000$, $\nu = 0.3$ and radius $r = 1$, pressed by a point load $F = 100$ onto a quadrilateral with material parameters $E = 10^6$, $\nu = 0.45$.

As is done in [CSW99], we apply the single load as surface load to avoid a singularity. Homogeneous Dirichlet boundaries have been applied on the right and left boundary part of the quadrilateral, see the right part of Figure 7.1. We use bilinear functions on quadrilaterals and uniform refinement. On both subdomains, we apply a $\mathcal{V}(3,3)$–cycle. In this example, we chose $\eta_1 = 1$ and $\eta_2 = 0.5$. The problems on the two subdomains are solved up to a tolerance of 10^{-10}. On each level, only a few outer iteration steps are required to reach the stopping criterion for $\varepsilon_{\mathrm{TOL}} = 10^{-5}$,

$$\frac{\|\mathbf{p}^\mu - S^T \mathbf{r}_1^\mu\|}{\|\mathbf{p}^\mu\|} \;\leq\; \varepsilon_{\mathrm{TOL}} \,.$$

In the left of Figure 7.3, the maximal contact stress on each level is displayed, showing the performance of our method. The analytical value of $\sigma_n^{\max} = 495$ is already reached on level 5. Here, only 5 nodes of the circle are actual in contact with the plane. In the middle of Figure 7.3, the contact and tangential stresses are shown, in the right, the component $\sigma_{22}(\mathbf{u})$ of the stress tensor is depicted. To demonstrate the flexibility of our approach, we do not enforce $\sigma_T = 0$ on the space. The Lagrange multiplier of the mortar method plays the role of the boundary stresses at Γ_C. Thus, the boundary stresses are handled as additional unknowns which can be obtained by a local post–processing from the residual. This observation predestinates our algorithm for contact problems with friction.

In our last example, we apply our algorithm to a more complex geometry. The elastic contact of a wrench and a nut is considered. At the interior boundary of the nut, i.e., the part of the boundary with outer normal pointing towards the center of gravity of the nut, we impose Dirichlet boundary conditions corresponding to a rotation by $\pi/180$. Homogeneous Dirichlet boundary conditions are applied at the handle of the wrench and on all remaining parts of the boundary we impose homogeneous Neumann conditions. We use linear elements on triangles, and adaptive refinement. The specified material parameters are $E = 7000$ and $\nu = 0.28$ and the damping parameters are $\eta_1 = 1$, $\eta_2 = 0.25$. As can be seen in the right of Figure 7.4, the actual

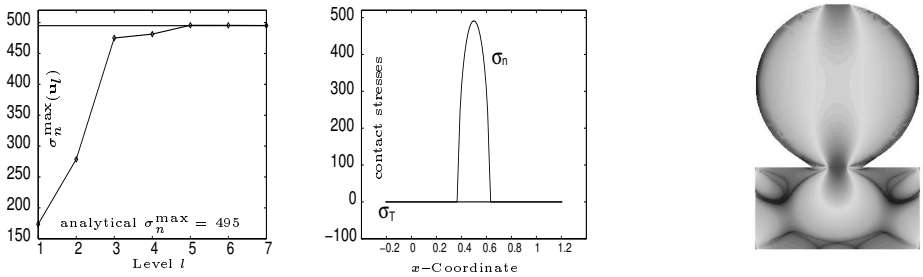

FIG. 7.3. *Maximal contact stresses (left), contact stresses (middle) and* σ_{22} *(right)*

contact zone is only a small part of the contact boundary Γ_C. We remark, that a more realistic model would include friction at the interface.

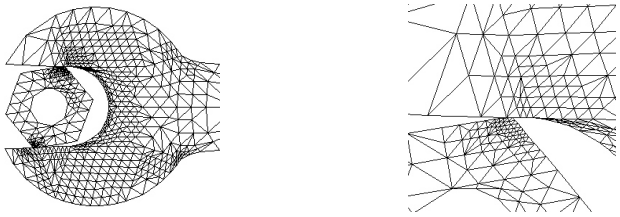

FIG. 7.4. *Details of the deformed configuration for the nonlinear contact problem*

REFERENCES

[BBJ+97] P. Bastian, K. Birken, K. Johannsen, S. Lang, N. Neuss, H. Rentz-Reichert, and C. Wieners. UG – a flexible software toolbox for solving partial differential equations. *Computing and Visualization in Science*, 1:27–40, 1997.

[BD98] D. Braess and W. Dahmen. Stability estimates of the mortar finite element method for 3–dimensional problems. *East–West J. Numer. Math.*, 6:249–263, 1998.

[Ben99] F. Ben Belgacem. The mortar finite element method with Lagrange multipliers. *Numer. Math.*, 84:173–197, 1999.

[BF91] F. Brezzi and M. Fortin. *Mixed and hybrid finite element methods.* Springer–Verlag, New York, 1991.

[BGK87] P. Boieri, F. Gastaldi, and D. Kinderlehrer. Existence, uniqueness and regularity results for the two–body contact problem. *Applied Mathematics and Optimzation*, 15:251–227, 1987.

[BM00] F. Brezzi and D. Marini. Error estimates for the three–field formulation with bubble stabilization. *Math. Comp.*, 2000. PII: S0025-5718(00)01250-3, March 24, 2000.

[BMP93] C. Bernardi, Y. Maday, and A.T. Patera. Domain decomposition by the mortar element method. In H. Kaper et al., editor, *In: Asymptotic and numerical methods for partial differential equations with critical parameters*, pages 269–286. Reidel, Dordrecht, 1993.

[BMP94] C. Bernardi, Y. Maday, and T. Patera. A new nonconforming approach to domain decomposition: The mortar element method. In H. Brezis and J. L. Lions, editors, *Nonlinear Partial Differential Equations and Their Applications*, pages 13–51. Pitman, 1994.

[CSW99] C. Carstensen, O. Scherf, and P. Wriggers. Adaptive finite elements for elastic bodies in contact. *SIAM J. Sci. Comp.*, 20(5):1605–1626, 1999.

[DNS99] Z. Dostal, F.A.M. Gomes Neto, and S.A. Santos. Solution of contact problems by FETI domain decomposition with natural coarse space projections. *Comp. Meth Appl. Mech. Eng.*, 1999. to appear.

[ESW99] C. Eck, O. Steinbach, and W.L. Wendland. A symmetric boundary element method

for contact problems with friction. *Mathematics and Computers in Simulation*, 50:43–61, 1999.

[Gop99] J. Gopalakrishnan. *On the mortar finite element method.* PhD thesis, Texas A&M University, August 1999.

[Hac85] W. Hackbusch. *Multi-Grid Methods and Applications.* Springer, Berlin, 1985.

[Her82] H. Hertz. Über die Berührung fester elastischer Körper. *J.f. Math.*, 92, 1882.

[HH80] J. Haslinger and I. Hlaváček. Contact between elastic bodies. I. continuous problems. *Apl. Mat.*, 25:324–327, 1980.

[HH81] J. Haslinger and I. Hlaváček. Contact between elastic bodies. II. finite element analysis. *Apl. Mat.*, 26:263–290, 1981.

[IHL88] J. Nečas I. Hlaváček, J. Haslinger and J. Lovíšek. *Solution of variational inequalities in mechanics.* Springer, Berlin, 1988.

[KK99] R. Kornhuber and R. Krause. On monotone multigrid methods for the Signorini problem. In W. Hackbusch and S.A. Sauter, editors, *Numerical Techniques for Composite Materials*, Proceedings of the 15th GAMM Seminar Kiel, 1999. in preparation.

[KK00] R. Kornhuber and R. Krause. Adaptive multigrid methods for Signorini's problem in linear elasticity. submitted, 2000.

[KLPV00] C. Kim, R.D. Lazarov, J.E. Pasciak, and P.S. Vassilevski. Multiplier spaces for the mortar finite element method in three dimensions. *Preprint, Texas A&M University*, 2000. submitted.

[KO88] N. Kikuchi and J.T. Oden. *Contact Problems in elasticity.* SIAM, Philadelphia, 1988.

[Kor97a] R. Kornhuber. *Adaptive monotone multigrid methods for nonlinear variational problems.* Teubner–Verlag, Stuttgart, 1997.

[Kor97b] R. Kornhuber. Adaptive monotone multigrid methods for some non–smooth optimization problems. In R. Glowinski et al., editor, *Domain Decomposition Methods in Sciences and Engeneering*, pages 177–191. Wiley, 1997.

[KW00a] R.H. Krause and B.I. Wohlmuth. Domain decomposition methods on nonmatching grids and some applications to linear elasticity problems. *submitted to ZAMM*, 2000.

[KW00b] R.H. Krause and B.I. Wohlmuth. Multigrid methods for mortar finite elements. In E .Dick, K. Riemslagh, and J. Vierendeels, editors, *Multigrid Methods VI*, volume 14 of *Lecture Notes in Computational Science and Engeneering*, pages 136–142, Berlin Heidelberg, 2000. Springer. Proceedings of the Sixth European Multigrid Conference Held in Gent, Belgium, September 27-30, 1999.

[PC99] G. Pietrzak and A. Curnier. Large deformation frictional contact mechanics: continuum formulation and augmented Lagrangian treatment. *Computer Methods in Applied Mechanics and Engeneering*, 177(3–4):351–381, 1999.

[Tal94] P. Le Tallec. *Handbook of Numerical Analysis*, volume III, chapter Numerical Methods for Nonlinear Three-Dimensional Elasticity. Nort–Holland, 1994. P.G. Ciarlet and J.L. Lions *(Eds.)*.

[WG97] K. Willner and L. Gaul. Contact description by fem based on interface physics. In *Computational Plasticity V*, Barcelona, Spain, 1997.

[WK01] B.I. Wohlmuth and R.H. Krause. Multigrid methods based on the unconstrained product space arising from mortar finite element discretizations. *to appear in SINUM*, 2001.

[Woh99a] B.I. Wohlmuth. Domain decomposition methods. Habilitationsschrift, Universität Augsburg, November 1999.

[Woh99b] B.I. Wohlmuth. A residual based estimator for mortar finite element discretizations. *Numer. Math.*, 84:143–171, 1999.

[Woh00] B.I. Wohlmuth. A mortar finite element method using dual spaces for the Lagrange multiplier. *to apear in SINUM*, 2000.

[Wri95] P. Wriggers. Finite element algorithms for contact problems. *Arch. Comp. Meth. Engrg.*, 2:1–49, 1995.